Universität Stuttgart

Institut für Energieübertragung und Hochspannungstechnik

Investigation of transformer behavior under dc influence with simulation models and laboratory measurements

Master thesis

by

David Velasco

Started:	28.10.2013
Finished:	26.05.2014
Supervisor:	M.Sc. Mario Gnädig

Clarification

I assure, that I performed and wrote this work on my own, except for the suggestions that my supervisor Mr. Mario Gnädig gave to me, and that I didn't use anything but the given sources and the sourced accessories.

Stuttgart, 26th May 2014

Ich versichere, dass ich die vorliegende Arbeit selbständig durchgeführt und verfasst habe, abgesehen von den Anregungen, die mir von Seiten meiner Betreuer Herrn Mario Gnädig gegeben worden sind und dass ich keine als die angegebenen Quellen und Hilfsmittel benutzt habe.

Stuttgart, 26. Mai 2014

Acknowledgements

Firstly, I would like to thank the Institut für Energieübertragung und Hochspannungstechnik (IEH) of the University of Stuttgart, for giving me the chance and the means to conduct this research during the academic year.

Special thanks to my supervisor Mr. Mario Gnädig, for his invaluable assistance from the very beginning until the end, despite the adversities along the way. His efficiency and many suggestions have been essential in the development of this work.

I would also like to thank my family and all of my friends who supported me towards my goal. Particular mention to my friend Iosu, whose encouragement, moral and priceless help during this period have left a big impression on me.

Abstract

The behavior of transformers under DC components has been since long studied. One of the principal sources of these components is the AC-DC energy conversion, in which unsymmetrical direct current components can arise. Another important phenomenon are the Geomagnetically Induced Currents (GIC), caused by an increased solar activity, which introduce an offset in the grounded neutral terminals of power transformers.

Among the literature there can also be found different investigations about the harmful effects that DC components may cause in power transformers [7] [8]. The presence of a DC component induces an offset on the flux flowing through the transformer core, which can lead the transformer into saturation. An increase on the magnetic field is immediate, and high associated magnetization currents appear. As a consequence of this, harmful harmonics and a distorted secondary voltage can also be observed. Furthermore, the increased magnetizing currents caused by the DC bias can lead to high leakage fluxes (increasing the losses) and localized hot spots on the tank walls [8].

Experimental setups and different measurements like the ones shown in this thesis can be useful in order to know in detail how the behavior of the transformer under DC influence is and which are the most harmful effects that may occur during transformer operation. Towards this purpose, a MATLAB-Simulink model for a three-phase three-limb transformer is introduced, and different simulations are carried out for a verification task.

Contents

Index of figures

Abbreviations

FEM: Finite Element Method
GIC: Geomagnetically Induced Currents
MMF: Magneto Motive Force
pu: per unit

Symbols

μ: Permeability
μ_0: Permeability of vacuum
A: Cross section of the iron core
B: Magnetic flux
H: Magnetic field strength
I_m: Magnetizing current
J: Magnetic polarization
l:Length of the iron core
L: Inductance
N_1: Number of turns of the primary winding
N_2: Numbers of turns of the secondary winding
P_0: No-load losses
P_c: Copper Losses in the transformer electrical windings
P_H: Hysteresis Losses
u_k: Short-circuit voltage
X: Reactance of the corresponding winding
Φ: Magnetic flux

$\hat{X}$: Values with this symbol refers to peak-amplitude values
X_1: Index “1“ refers to primary side values
X_2: Index “2“ refers to secondary side values

Introduction

The main goal of this thesis is to investigate the effects of DC components on transformers and the power network. In order to achieve this goal, several tasks regarding literature research and transformer modelling were performed in first place. Afterwards, a development of a proper laboratory setup and a detailed analysis of the measurement results were carried out, so that the behavior of this setup could be verified with the MATLAB-Simulink model.

A good understanding of the Simulink model used along this thesis has been of key importance in order to carry out the simulations, adjusting the model parameters and solving the different issues that showed up throughout the performance of this work. However, the measurements carried out in the laboratory are considered to play an essential role, since they reflect the real behavior of a transformer under DC influence and therefore allow the verification of the MATLAB model, which is set as one of the goals of this work.

As a sum-up of the main aims of the thesis, the following points are highlighted:

- Integration of a comprehensive three-phase three-limb transformer model in the MATLAB-Simulink environment.
- Arrangement of a laboratory setup in order to carry out the measurements, obtain the transformer parameters and apply them afterwards to the MATLAB model.
- Performance of the proper comparisons between the model simulations and the measurements, in order to verify the model and know its limitations.
- Investigation and understanding of the transformer and power network behavior under DC excitation.

Regarding the outline of the work, the MATLAB model for the transformer used in the experimental setup is introduced in Chapter 1, while the main characteristics of the transformer and some overview concerning its geometry and construction is presented in Chapter 2.

Afterwards, some of the measurements carried out in the laboratory are shown in Chapter 3. These measurements comprise no-load tests, short-circuit test and hysteresis tests.

The data extracted from these measurements is then properly processed in order to obtain the main parameters of the real transformer, and consequently be able to introduce them into the model. This matters are dealt in Chapter 4.

Once the implementation of the parameters is done, different simulations under operating conditions are carried out in the model, and a detailed comparison between them and the measurements is presented. This can be found in Chapter 5.

Chapter 6 introduces the second and final part of the thesis, in which the behavior of the transformers under DC influence is analyzed. Different scenarios are proposed and a comparison between simulation results and measurements is shown.

Future works are proposed in the outlook shown in Chapter 7, while Chapter 8 shows the Appendix where documentation related to the work can be found. Eventually, Chapter 9 comprises an index of the literature used.

1 Introduction of the MATLAB model

In the first section of this chapter, the MATLAB model is introduced. Afterwards, the main parameters that this model requires are presented, followed by a description of the way the model is controlled.

1.1 Model description

The three-phase transformer model taken as the starting point in this work was developed by Sybille Gilberth (Hydro-Quebec, IREQ) and is provided in the MATLAB-Simulink environment.

The model is divided in different layers. The general layer shows the disposition of the power supply, the transformer, the electrical elements of the grid, measurement stations and the load. In this first layer, the main parameters of the transformer as well as initialization values can be set by means of an interface.

The modelling of the electrical windings can be found in the second layer. The main inductance of the transformer is modelled as a controlled current source, which depends on the state of the magnetic circuit, found in a third layer. It is important to highlight, that the electric and magnetic circuit are modelled separately, but are strongly linked, as will be described further on.

The model consists therefore of two inter-connected blocks:

- An electrical circuit, which models the electrical properties of the transformer
- A magnetic circuit, which models the magnetic properties.

Regarding the winding distribution and the iron core structure, a three-phase two-winding core-type transformer is considered. The iron core is composed, thus, by three limbs bearing the coils, two per limb, and four yokes that interconnect them, as is represented in Figure 1. Phases R and T are wound on the external limbs, while phase S is wound on the central limb.

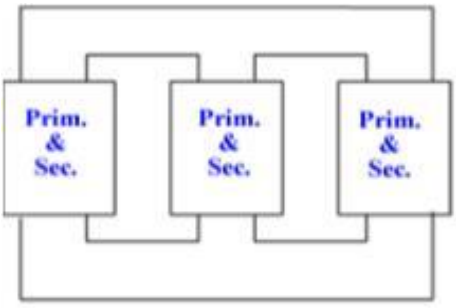

Figure 1: Electrical winding distribution in the transformer

As it is explained later on, the magnetic core geometry and the iron B-H characteristics are also integrated in this model. In order to describe how the electrical and magnetic circuits are modelled, a look under the transformer mask is taken. As can be seen in Figure 2, the electrical

circuit is implemented by six controlled current sources, one per winding. These current sources are ruled by the MMF developed from each winding.

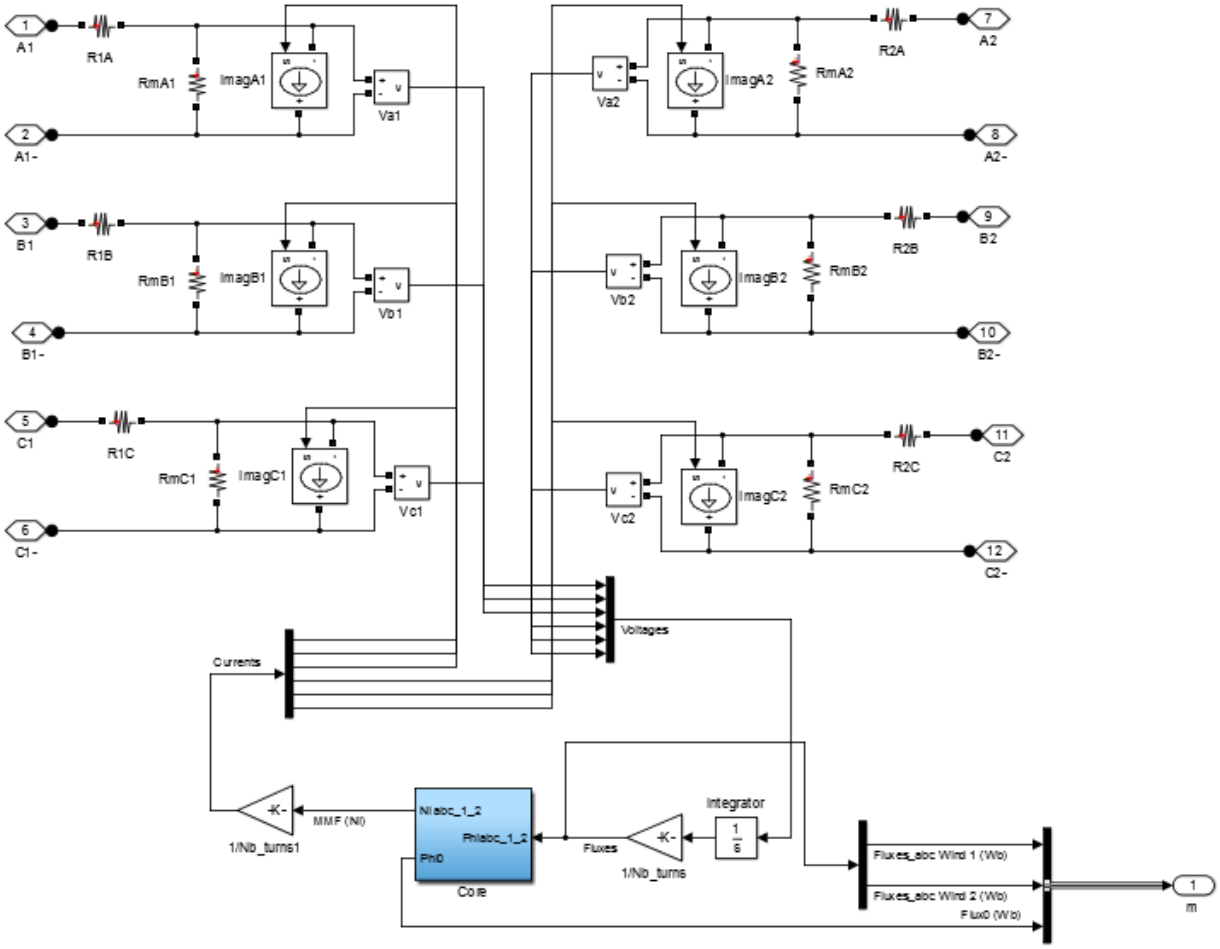

Figure 2: Electrical subsystem of the MATLAB model

The magnetic core subsystem uses the electric-magnetic analogy to implement the magnetic circuit shown in Figure 3, which consists of 7 iron elements: 3 limbs and 4 yokes, which appear in blue in the figure, and 7 air elements (in green) representing flux leakages for each of the six coils and a zero-sequence flux return path.

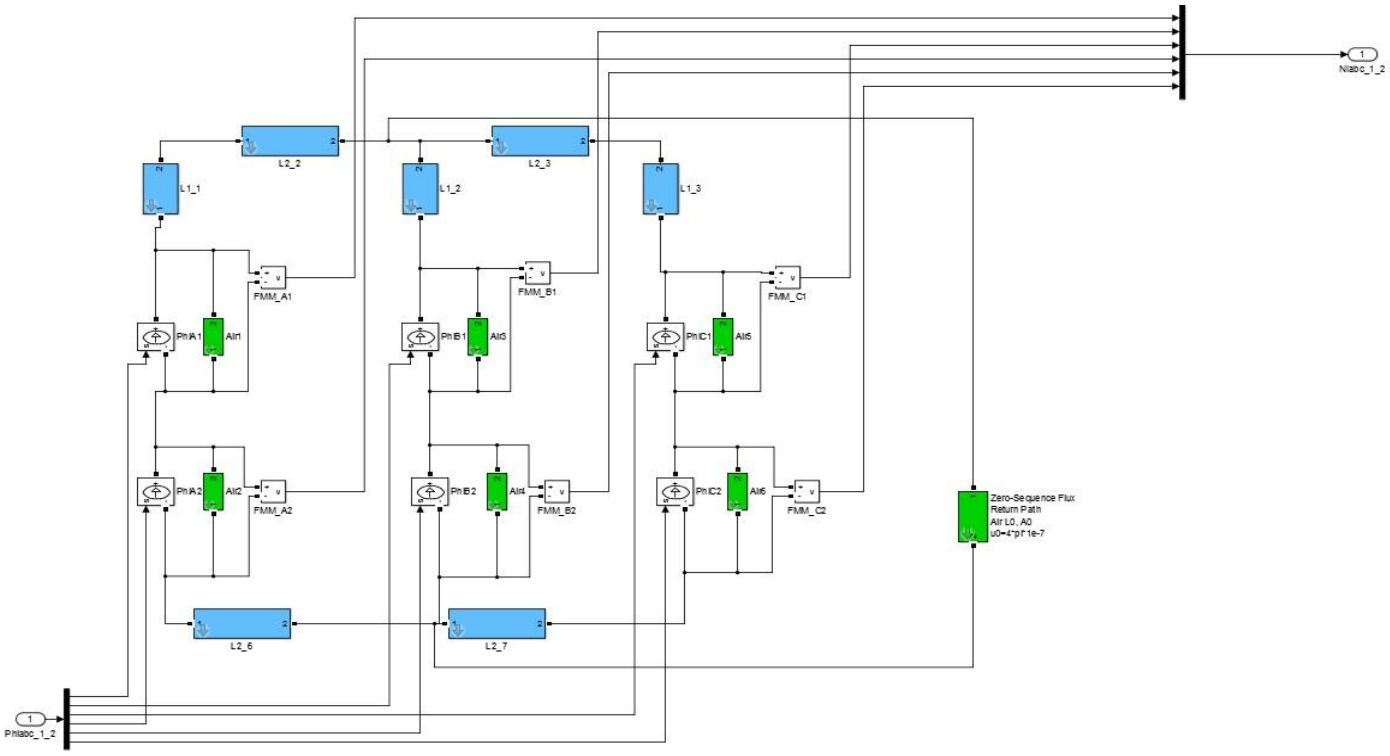

Figure 3: Magnetic subsystem of the MATLAB model

1.2 Model Parameters

The most important parameters used by the model for its computations are shown in Table 1.

Table 1: Parameters implemented in the MATLAB model

	Symbol
Resistance of winding i	R_i
Real power losses in Iron	P_o
Leakage reactance of winding i	x_i
Average length of limbs and yokes	L
Effective section of limbs and yokes	A
Weight of limbs and yokes	$W_{L,Y}$
BH Characteristic of Iron Core	Look-up Table

R_i is the resistance of the corresponding winding of phase i, whereas x_1 and x_2 are the leakage reactances of the primary and secondary winding, respectively. By means of a short-circuit test, these reactances can be obtained. The scenario that considers the model for this purpose is represented in the figure below.

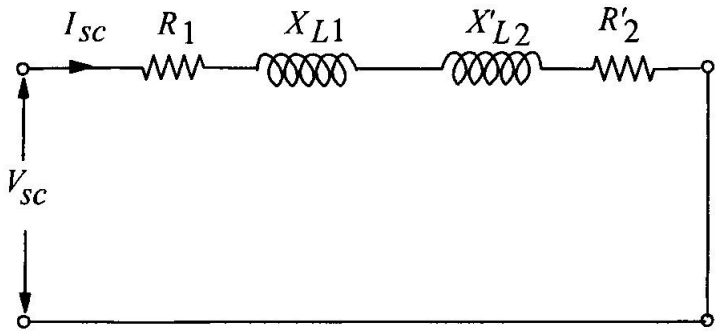

Figure 4: Short-circuit test equivalent circuit

In order to understand the computations that the model carries out, it must be noticed that both the magnetizing reactance X_M in parallel with the resistance R_{Fe} that models the iron losses in a standard equivalent circuit, are in this scenario neglected, since $R_{Fe}||X_M \gg X_{L2}{}' \cdot R_2{}'$. As a simplification, the pu value of the copper resistances is considered negligible compared to the reactances x [2]. The rated current of 1 pu value that flows during this test, implies that half of the pu voltage u_k is equal to each of the leakage reactances, as they are considered of the same value. Therefore, the leakage inductance value of the limbs is computed now by the model as shown in Formulas (1)-(3). In Section 8.1 of the Appendix, the exact code implemented in the model can be found.

$$x_1 = \frac{u_k}{2} \tag{1}$$

$$x_2 = x_1 \tag{2}$$

$$L_1 = x_1 \cdot \frac{{U_1}^2}{P_n \cdot 2\pi \cdot f_n} \tag{3}$$

1.3 Model Operation Description

The basic principles about how the Simulink model operates are introduced in this section. Nevertheless, the reader can find among the related literature deeper explanations [5].

As a first step, the voltage in the primary winding is set. This voltage has, according to the basic electromagnetic law of induction applied to inductors with a fixed numbers of turns shown in Formula 4, a related variation of flux inside the magnetic core.

$$V = N\frac{d\phi}{dt} \tag{4}$$

This variation of flux is computed by the model integrating the voltage with the proper initial conditions set on the fluxes of each phase, as shown in Formula 5.

$$\phi_{0,i,primary} = \frac{-V_0 \cdot \sqrt{2}}{2\pi f_n \cos(\theta_i)} \qquad \boldsymbol{i} = \mathbf{r, s, t} \tag{5}$$

These initial conditions are obtained integrating the three-phase sinusoidal voltages and imposing the boundary zero-offset condition for the fluxes. The secondary initialization fluxes are computed through the voltage ratio, as shown in Formula 6.

$$\phi_{0,i,secondary} = \phi_{0,i,primary} \frac{U_2}{U_1} \qquad \boldsymbol{i} = \mathbf{r}, \mathbf{s}, \mathbf{t} \tag{6}$$

It must be noticed that the computation shown in Formula 6 is only valid if no phase-shift between the voltages of the primary and secondary side is considered.

The MMF associated to these alternating fluxes is measured in the magnetic circuit, and is divided then by the number of turns. This value, $\frac{Mmf}{N}$, is recirculated to the electrical circuit of the corresponding winding.

The fluxes, minus the corresponding leakage fluxes associated to each winding, flow in the model through each limb and yoke of the magnetic circuit. These limbs and yokes have a reluctance value, which opposes to the flowing flux and produces consequently a MMF drop.

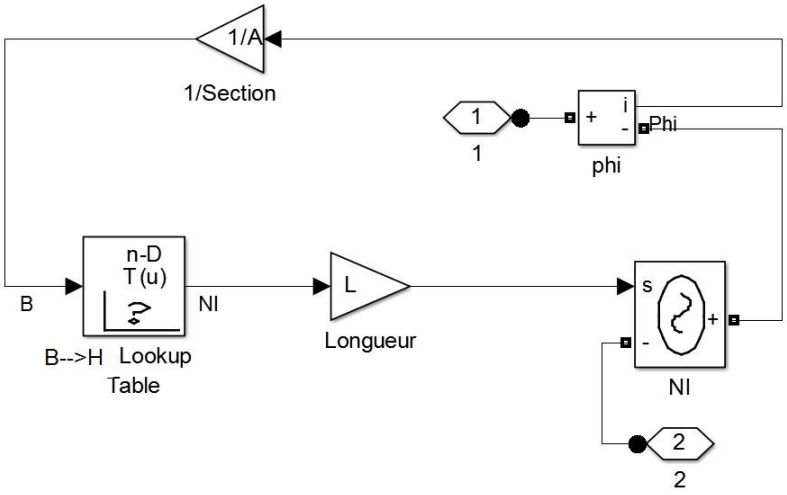

Figure 5: Limb/yoke magnetic circuit

As can be seen on Figure 5, the flowing flux is divided by the effective cross section of the iron core, obtaining the magnetic flux density B. Then, by means of the manufacturer B-H table, the magnetic field strength H is computed. According to Formula 7, when this value is multiplied by the length of the magnetic path, results into a MMF drop.

$$HL = NI = MMF_{drop-\text{limb/yoke}} \tag{7}$$

The zero-sequence path resistance is also modelled. Under balanced conditions, the zero-sequence component should be zero. However, the magnetic core is not perfectly symmetric, as the flux path for the outer limbs is longer than the path for the central limb. As a result, the sum of the three-phase fluxes can be different from zero and must close his path through the air or the tank, when exists. Due to the high magnetic reluctance of the air, high zero-sequence

excitation currents are required in order to find a significant zero-sequence flux. Under unbalanced conditions, as will be seen later with the DC analysis, this zero-sequence flux increases.

Regarding the power losses, the MATLAB model computes the losses in each of the segments in which the iron core is divided. The input parameter in this computation is the simulated magnetic flux density B within the core segment.

Figure 6: Simplified iron losses computation by the model for a core segment

The maximum and minimum values of the B value is related to a certain value of loss per kg, specified by the iron manufacturer. These correlation is implemented in the model through a "Look-up" table, as shows Figure 6, and eventually the power losses per kilogram are multiplied by the mass of the core segment. For further details, among the literature can be found deeper description of these computations [5].

2 Real transformer description

As mentioned before, an essential part of this thesis is the correct computation of the different parameters of the transformers, since the accuracy of the simulations will strongly depend on this. The following chapter focuses on the different features of the real transformer used in this work.

Table 2: Parameters implemented in the MATLAB model

	Symbol	
Resistance of winding i	R_i	
Real power losses in Iron	P_o	
Short-circuited voltage (pu)	u	
Average flux path length of limbs and yokes	L	
Effective section of limbs and yokes	A	
Weight of limbs and yokes	$W_{L,Y}$	
BH Characteristic of Iron Core	Look-up Table	

The important parameters required by the MATLAB model are sum up in Table 2: Parameters implemented in the MATLAB model. Since both transformers have the same features, the measurements are carried out in only one of the two transformers.

2.1 Transformer characteristics

In Table 3, a list of the main characteristics given by the transformer manufacturer is shown.

Table 3: Transformer characteristics

Rated Power	$2\ kVA$	
Rated Voltage	$400\ V\ AC$	
Frequency	$50\ Hz$	
Number of primary turns	277	
Number of secondary turns	286	
Rated primary current	$I_{1N} = 2.98\ A$	
Rated secondary current	$I_{2N} = 2.89\ A$	
Winding voltage feasible ratios	400/400 400/266 400/200	
Connection between windings	Star-Star	
Neutral	Brought out to terminals	
Phase shift between primary and secondary	0º	

Power losses at rated conditions	$83\ W$	
Number of limbs	3	
Weight of the iron core	$13.3\ kg$	
Maximum B_0	Not given	

2.2 Geometry and construction of the iron core

A brief information regarding the iron core geometry and construction is introduced in this section.

2.2.1 Geometry of the iron core

The geometry of the iron core given by the manufacturer can be seen in Figure 7, where all lengths are expressed in mm.

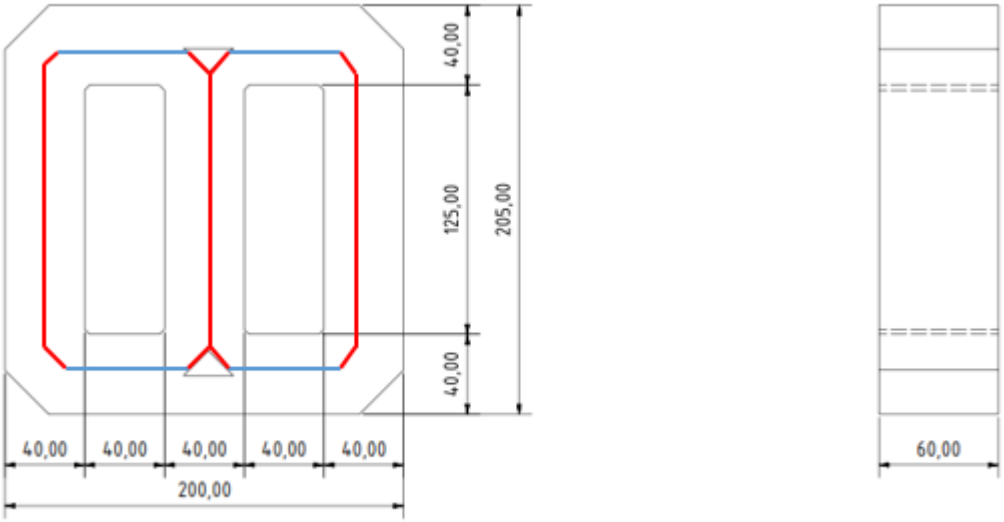

Figure 7: Iron core geometry. Values given in mm

From this data, the parameters listed below can be computed:

- Geometrical core cross section: $A = 2400\ mm^2$
- Length of the main path:
  - Limb i: $L_i = 205 - 40 - 2 \cdot 10 + 2 \cdot 10 \cdot \sqrt{2} = 173.28\ mm$
  - Yoke i: $Y_i = 40 + 10 + 10 = 60\ mm$

Using the iron density $\rho = 7.65 \frac{kg}{dm^3}$, obtained from [1], and the total weight of the core structure, given by the manufacturer, the exact volume of the core can be calculated as follows:

$$vol = \frac{mass}{density} = \frac{13{,}3\ kg}{7.65\ \frac{kg}{dm^3}} = 1.74\ dm^3 \quad (8)$$

Volumes can be also be computed by means of the geometry of the core. Formulas 9-11 show the results.

$$volume\ of\ the\ three\ limbs = 1.25\ dm^3 \quad (9)$$

$$volume\ of\ the\ three\ yokes = 0.58\ dm^3 \quad (10)$$

$$total\ volume = 1.82\ dm^3 \quad (11)$$

The slight discrepancy between the value for the iron core volume obtained in Formula 8 and the one obtained in Formula 11 suggests the existence of error in the core geometry computations. In Formulas 12 and 13, the mass of the limbs and yokes is calculated in order to implement them in the model.

$$mass\ of\ each\ limb = density \cdot volume\ of\ each\ limb = 3.1814\ \text{kg} \quad (12)$$

$$mass\ of\ each\ yoke = density \cdot volume\ of\ each\ yoke = 1.1016\ \text{kg} \quad (13)$$

The model requires these values in order to compute the iron losses in each of the segments in which the iron core is discretized.

2.2.2 Construction

The transformer iron core is generally composed of many layers, as illustrates Figure 8, with a thickness generally between 0.20 and 0.5 mm [2], with the purpose of preventing big eddy currents.

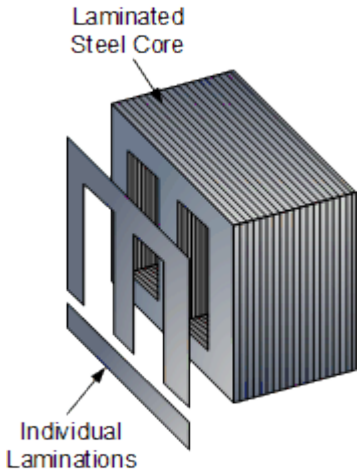

Figure 8: Iron core construction

Due to this fact small gaps can be found in between these layers, and consequently, the effective cross section of the iron core shall be considered smaller than the one given in the core geometry. In order to take this into account, a minimum stacking factor is obtained from the

iron manufacturer. The factor of 96% [1] is multiplied in Formula 14 by the geometric area computed in the previous section.

$$A_{eff} = A_{geom} \cdot k = 2400 \cdot 0.96 = 2304\ mm^2 \quad \textbf{(14)}$$

In order to reduce the magnetic losses and increase consequently the efficiency of the transformer, the manufacturer minimizes the quantity of iron used in the core structure. However, as a consequence of this, the transformer is found to be appreciably saturated during its operation under rated conditions, increasing therefore the iron losses per kilogram unit.

3 Laboratory measurements

3.1 Winding resistances

In first instance, a measurement of each electrical winding resistance of the transformer is carried out. As a first approach, the resistances are measured directly with an Ohmmeter. Secondly, the scenario shown in Figure 9, which corresponds to the Voltage-Current Method, is considered.

As can be seen in Table 4, each resistance value measured with the Ohmmeter results equal in all phases.

Table 4: Resistances values measured

	Phase R	Phase S	Phase T	Average value	Way of measuring
Primary side	0.8 Ω	0.8 Ω	0.8 Ω	0.8 Ω	Ohmmeter
Secondary side	1.00 Ω	1.00 Ω	1.00 Ω	1.00 Ω	
Primary side	0.85 Ω	0.84 Ω	0.84 Ω	0.84 Ω	Voltage-Current Method
Secondary side	1.12 Ω	1.12 Ω	1.12 Ω	1.12 Ω	

Thus, a DC current of about 1.7 A is injected through each winding resistance by means of a DC current source, and the voltages between terminals of the different windings are measured.

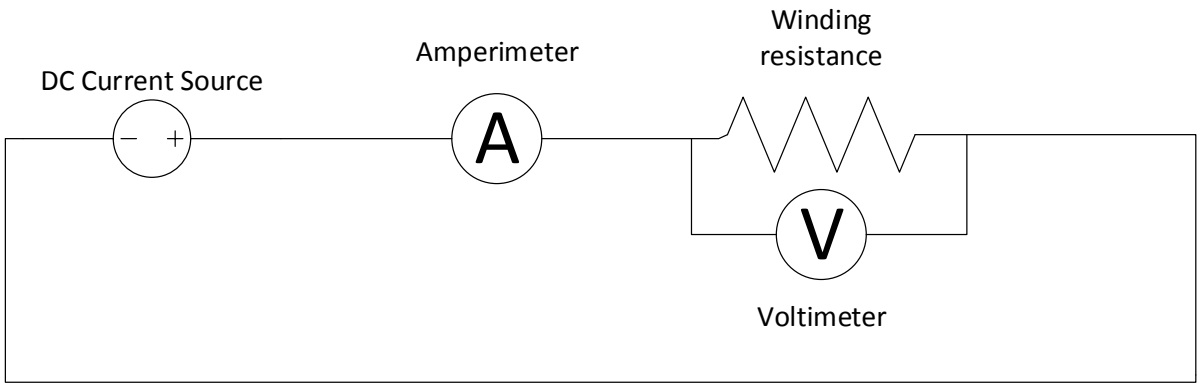

Figure 9: Voltage-Current method

Regarding

$$R = \frac{V}{I} \tag{15}$$

the different values are computed and shown in Table 4. The reader can notice that these values are close to the ones measured directly with the Ohmmeter.

As the MATLAB model considers one value for the primary and secondary side respectively, the average values shown in Table 4 will be afterwards implemented.

3.2 No-load test

After measuring the resistance of the windings, a no-load test is carried out, in order to compute the no-load losses of the transformer.

Rated voltage is supplied from the network grid to the transformer, obtaining the currents shown in Figure 10 and the real power consumption shown in Figure 11. The power losses value for each phase appear in Table 5.

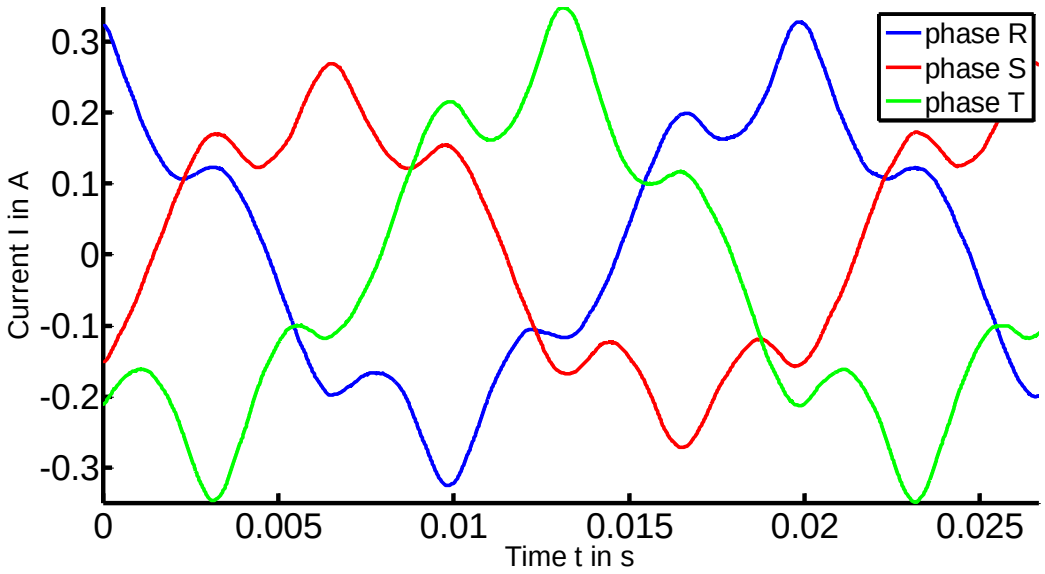

Figure 10: Primary currents during a 230 V no-load test

As can be easily seen in Figure 10, the primary currents show a strong 3th harmonic component. This event suggests that under rated conditions, the transformer is operating somewhere in the saturated region. This fact is of key importance, as further steps shown in this thesis will be made taking this into account. Another appreciable phenomenon is the lower amplitude showed by the central phase, compared to the external ones. This result is expected, as the central limb of the iron core structure needs less current in order to be magnetized, due to its shorter magnetic path length compared to the ones of the other phases.

Table 5: Power consumption during no-load test

Average Power of phase R	9.55 W
Average Power of phase S	3.87 W
Average Power of phase T	12.88 W
Total sum	26.30 W

These losses correspond to the sum of the copper losses and iron losses. However, due to the small magnetizing currents flowing during the test, the copper losses can be neglected. An asymmetrical power lecture can be observed.

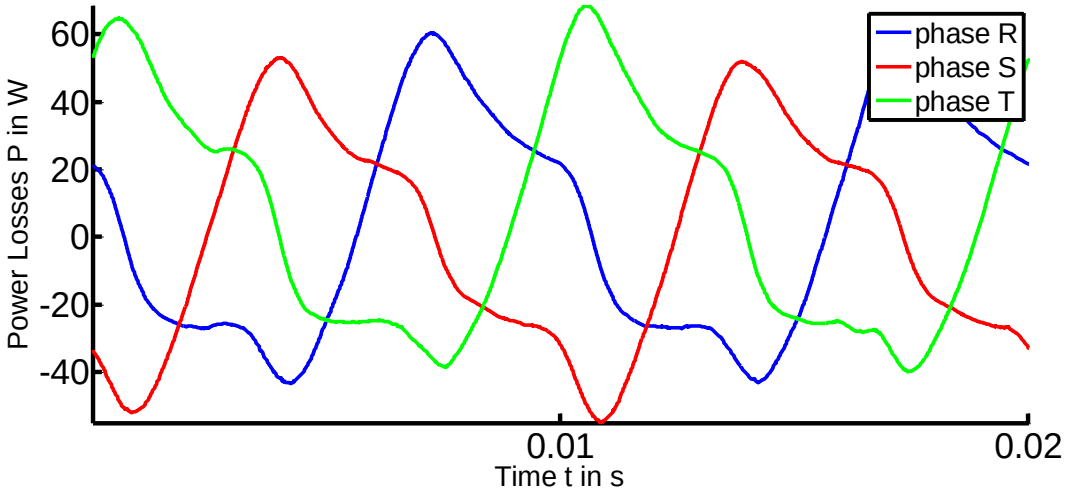

Figure 11: Power losses in the three phases during no-load test measurement

Taking a look now to the total losses value given by the manufacturer, it can be said that the iron losses during rated voltage must be approximately equal to the total power losses in rated conditions (with rated current) minus the copper losses:

$$P_{iron} = P_{total} - P_{cu} = P_{total} - \sum_{i=1}^{3} {I_{1,i}}^2 \, \mathrm{R}_1 - \sum_{i=1}^{3} {I_{2,i}}^2 \, \mathrm{R}_2 =$$

$$= 83 - 3 \times 2.98^2 \times 0.845 - 3 \times 2.89^2 \times 1.125 =$$

$$= 83\ \mathrm{W} - 22.51\ \mathrm{W} - 28.19\ \mathrm{W} = 83\ \mathrm{W} - 50.7\ \mathrm{W} = 32.3\ \mathrm{W}$$

Taking into account that the power losses in the iron during rated conditions are not perfectly equal to the ones during a no-load test, and the measurement errors, it can be stated that both values, the one computed from the manufacturer data and the one measured on the no-load test, match well with each other.

In order to know the variations on the transformer power consumption under no-load conditions, different voltages are supplied by means of a step-up transformer, and the real power is computed on each test. The setup used during the no-load tests performance is illustrated in Figure 12, and the power losses for different voltages is shown in Figure 13.

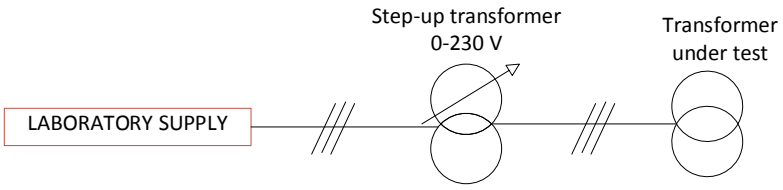

Figure 12: No-load test setup connection diagram

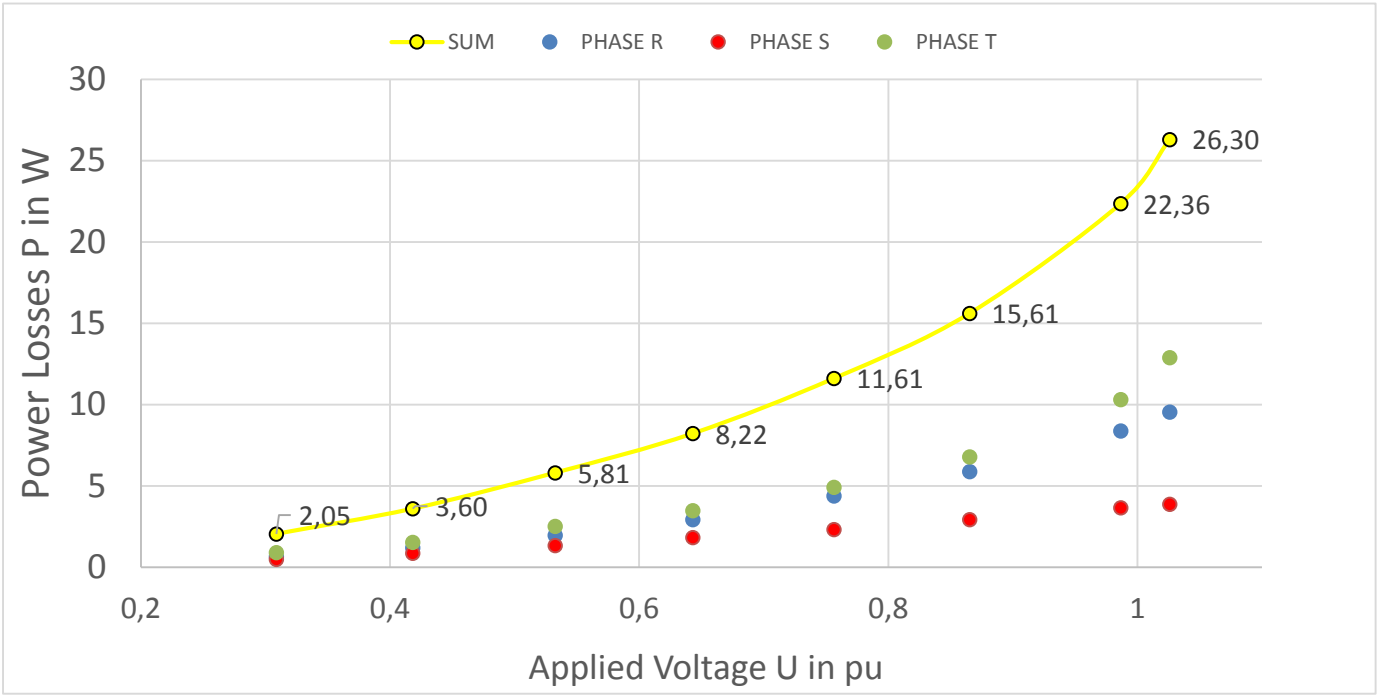

Figure 13: Primary phase-to-ground voltage applied against power losses in the three phases during no-load test measurements

Although power in phase T is always higher than the one in phase R, both powers seem to have the same trend, which can be followed by a polynomial of order 2, according to the fact that the iron losses are proportional to the squared voltage applied.

Phase S power tendency, however, seem to be different. This power keeps for all voltages lower than the ones on the other phases, and its increasing rate is quite lower. This fact can also be expected, if it is taken into account that the magnetic path of this central phase is shorter and therefore, less current is needed in order to magnetize this phase. The measured current results lower in amplitude, and the power is consequently lower than in the other phases too.

Different works can be found among the literature rewarding no-load test measurements, with special mention to non-equal power lectures among phases. As a sum up of the main reasons of this phenomenon, the following points are highlighted, according to [3]:

- The different number of turns in each phase, the asymmetrical disposition of the three windings along the iron core and its dimensions and layout results into asymmetrical

mutual impedances between phases. This results into unbalanced currents and contributes strongly to the non-equal power reading.

- The stray losses produced by each phase are not equal, and this produce an increase on the already existent asymmetry.
- Another contributor to this phenomenon is the angle difference that may exist between voltages of the three phase supply from 120º. Depending on this difference, the final effect could be either more or less strong. The angle deviation from $120°$ seen on this test is within $\pm 0.2°$.

Besides the contributors mentioned above, this phenomenon gets emphasized in transformers whose yoke length is quite appreciable as compared to limb heights, as this increases the asymmetry between the middle and outer phases [2]. These average lengths were computed in section 2.2.1 for the laboratory transformer, and are the following:

- Limbs: $L_{average} = 173.28\ mm$
- Yokes: $Y_{average} = 60\ mm$

3.2.1 Power supply analysis

During the no-load test seen at the beginning of this chapter, a non-perfect sinusoidal voltage supply is observed. As mentioned before, this may be in some cases another important factor that contributes to non-symmetrical power losses.

As shown in Figure 14, the voltage supplied by the step-up transformer used in Section 3.2 and further on, is distorted in an appreciable way. This fact has been taken into account for future measurements.

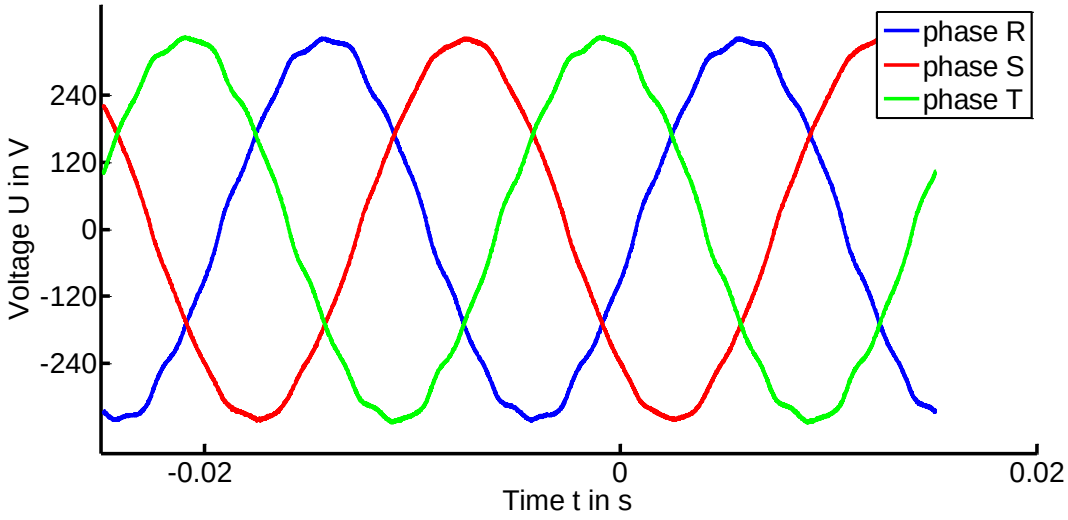

Figure 14: Voltage supplied by the step-up transformer used along the work

3.3 Short-circuit test

After the no-load test measurements, a short circuit test is carried out, in order to obtain the short-circuit voltage value, required by the model. The setup used during the short circuit test performance is also the one shown in Figure 12 of the previous section. In order to obtain more balanced voltages, and, therefore, more accurate results, a more stable step-up transformer than the one used for the no-load test is chosen. For the lower voltages required by this test, the previous transformer provided distorted and unbalanced supply that affected negatively to the results.

Once the secondary windings are short-circuited, the pertinent measures are taken.

Figure 15: Short-circuit test setup

The setup used for this test can be seen in Figure 15, and the simplified circuit shown in Figure 16 is the one considered for the test. The short-circuit voltage applied on the primary side makes rated current flow through the windings, when the secondary side is short-circuited.

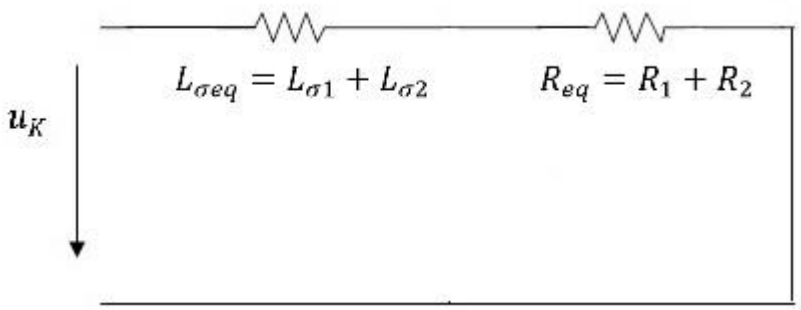

Figure 16: Short-circuit test equivalent circuit

The total short-circuit loss is composed of the copper losses caused by the rated current flowing though the resistances, and the losses associated to the leakage fluxes.

The voltages and currents obtained in this test are shown in Figure 17 and Figure 18.

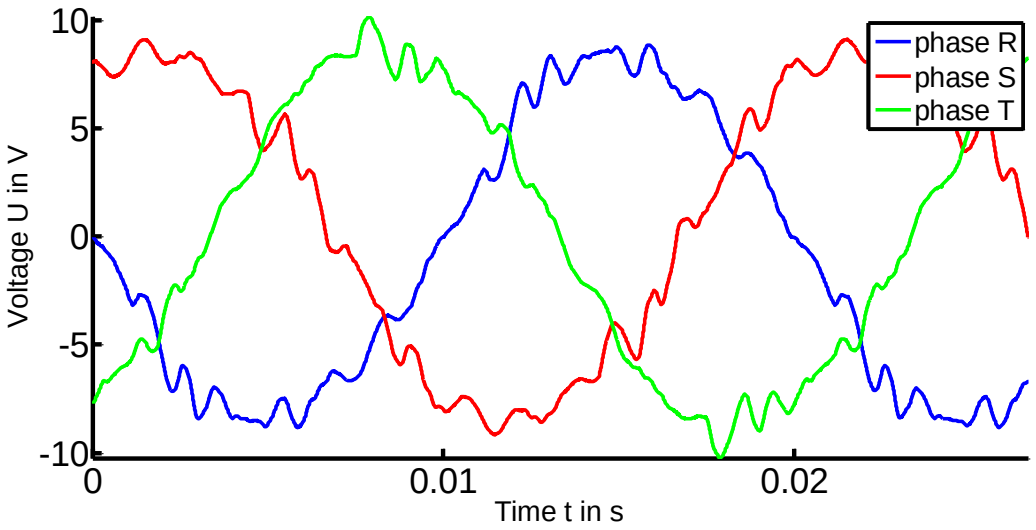

Figure 17: Primary phase-to-ground short-circuit voltages

At these small voltage levels, the feeding transformer provides an unbalanced and distorted voltage supply. Due to this fact, it can be seen in Figure 18 that the current of phase T is slightly higher than in the other phases.

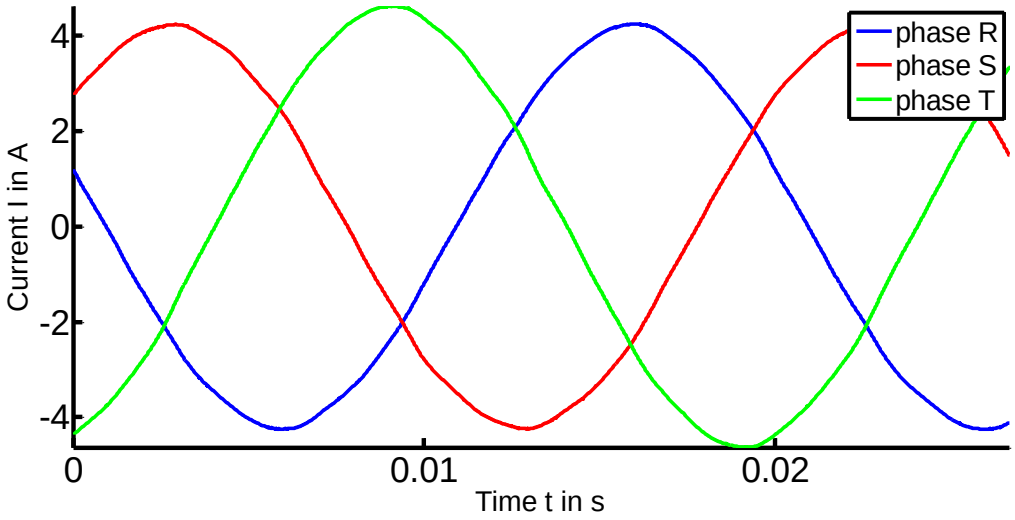

Figure 18: Secondary short circuit currents

As far as the computations are concerned, the pu short-circuit voltages are calculated in Formulas 16-18.

$$u_{kRm} = \frac{U_k}{U_N} = \frac{8.865 \cdot \sqrt{3}}{\sqrt{2} \cdot 400} = 0.0271 \quad (16)$$

$$u_{kSm} = \frac{U_k}{U_N} = \frac{9.116 \cdot \sqrt{3}}{\sqrt{2}400} = 0.0279 \quad (17)$$

$$u_{kTm} = \frac{U_k}{U_N} = \frac{10.178 \cdot \sqrt{3}}{\sqrt{2} \times 400} = 0.0312 \quad (18)$$

As the measured current I_m is in each phase slightly different to the rated current I_N, the correction factor $\delta = \frac{I_N}{I_m}$ is defined and applied to the computations, in order to obtain a more precise short-circuit voltage.

$$u_{kR} = u_{kRm} \cdot \delta_R = 0.0271 \frac{2.89}{\frac{4.09}{\sqrt{2}}} = 0.0271 \quad (19)$$

$$u_{kS} = u_{kSm} \cdot \delta_S = 0.0279 \frac{2.89}{\frac{4.08}{\sqrt{2}}} = 0.0279 \quad (20)$$

$$u_{kT} = u_{kTm} \cdot \delta_T = 0.0312 \frac{2.89}{\frac{4.39}{\sqrt{2}}} = 0.0290 \quad (21)$$

$$P_{kR} = P_{kRm}(\frac{I_N}{I_{Rm}})^2 = 17.212\ (\frac{2.89}{\frac{4.09}{\sqrt{2}}})^2 = 17.219 \quad (22)$$

$$P_{kS} = P_{kSm}(\frac{I_N}{I_{Sm}})^2 = 17.662\ (\frac{2.89}{\frac{4.08}{\sqrt{2}}})^2 = 17.696 \quad (23)$$

$$P_{kT} = P_{kTm}(\frac{I_N}{I_{Tm}})^2 = 19.827\ (\frac{2.89}{\frac{4.39}{\sqrt{2}}})^2 = 17.214 \quad (24)$$

According to [2], taking the leakage reactance value X as the impedance value Z may not be true for small distribution transformers. Therefore, the resistances and the copper losses associated to them are taken into account in the calculations.

$$u_{RLosses} = \frac{P_{kR}}{S_R} = \frac{17.219}{\frac{2000}{3}} = 0.0258 \quad (25)$$

$$u_{SLosses} = \frac{P_{kS}}{S_S} = \frac{17.696}{\frac{2000}{3}} = 0.0265 \quad \textbf{(26)}$$

$$u_{TLosses} = \frac{P_{kT}}{S_T} = \frac{17.214}{\frac{2000}{3}} = 0.0258 \quad \textbf{(27)}$$

In Formulas 25-27 the ohmmic components are computed. From this values, the inductance component values are obtained, as show Formulas 28-30.

$$u_{xR} = \sqrt{{u_{kR}}^2 - {u_{RLosses}}^2} = 0.0084 \quad \textbf{(28)}$$

$$u_{xS} = \sqrt{{u_{kS}}^2 - {u_{RLosses}}^2} = 0.0087 \quad \textbf{(29)}$$

$$u_{xT} = \sqrt{{u_{kT}}^2 - {u_{RLosses}}^2} = 0.0133 \quad \textbf{(30)}$$

As the MATLAB model considers only one short-circuit voltage value in order to compute the inductances of the transformer, an average value is computed in Formula 31. The leakage inductances are different in each phase of the real transformer, and the stray losses too. Taking an average value, the reader must notice that this asymmetry is not being represented in the model.

$$u_{k\,av} = 0.0085 \quad \textbf{(31)}$$

For the calculation, only phase R and S are taken into account. Phase T supply showed a deviation, as seen before, and therefore the computed value for this phase, which differs significantly from the ones obtained in the other phases, is not taken into account.

3.4 Hysteresis test

After the short-circuit test measurements, a hysteresis measurement is carried out. For this purpose, the transformer is fed by the step-up transformer, and its secondary side is kept opened. Then, the voltage on the secondary side and the excitation current on the primary side are measured.

Two different voltages, 230 V (rated supply) and a lower one, 140 V, are considered. The test results can be observed in Figures 19 and Figure 20.

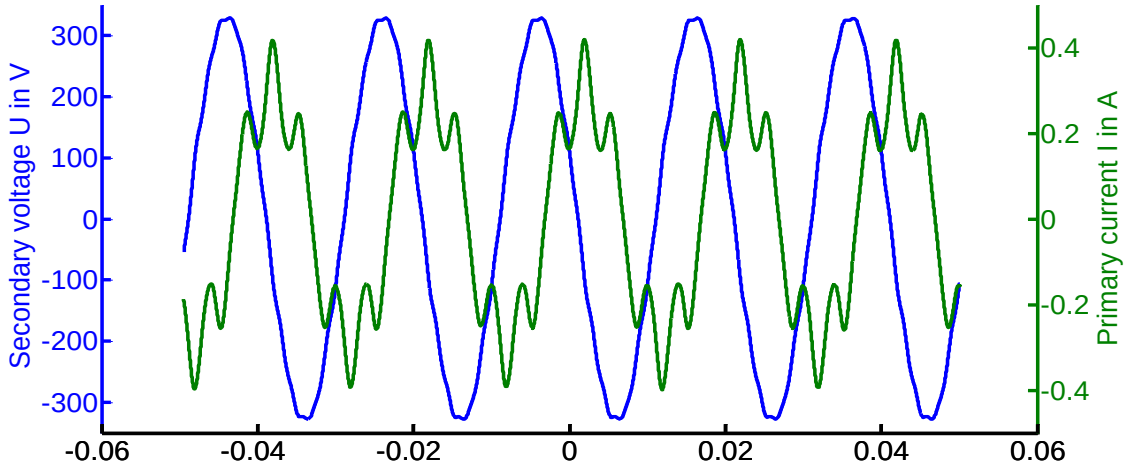

Figure 19: Secondary voltages and primary currents in a 230 V hysteresis test

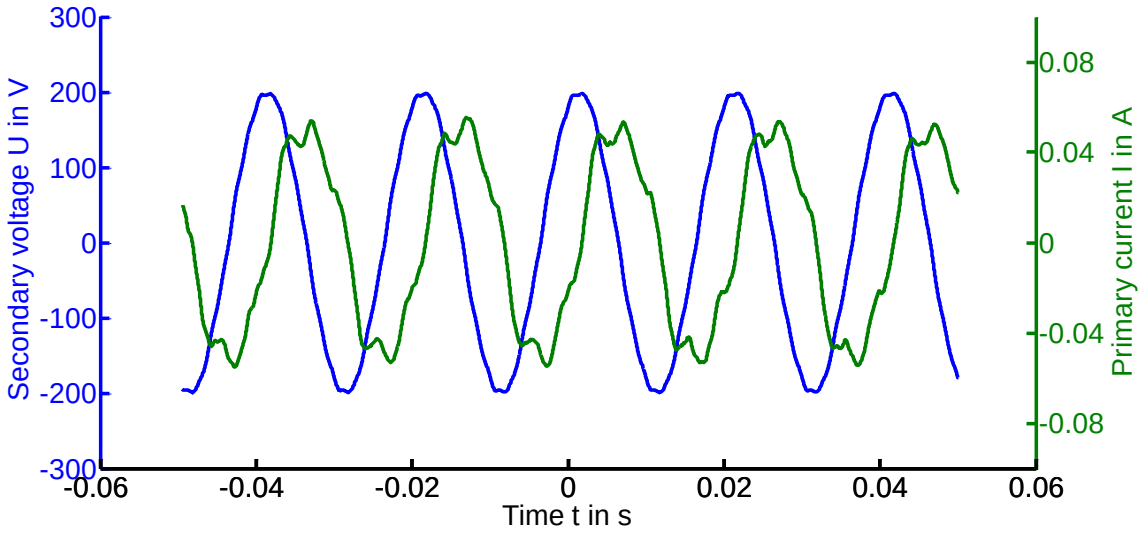

Figure 20: Secondary voltages and primary currents in a 140 V hysteresis test

The currents in Figure 19, which correspond to a voltage supply of 230 V, show that the transformer is working deep in the saturation region. Applying a lower voltage, as the one of Figure 20, can be seen that the currents are only slightly distorted, which indicates that the transformer is approaching the saturation region, somewhere close to the knee point of any standard BH Curve.

In order to obtain an approximate value of the fluxes, an integration through MATLAB of the secondary voltage over a $2T$ period time is carried out.

$$\frac{\int U dt}{A\,N} = \frac{\phi}{A} = B \tag{32}$$

$$H\,L = N\,i \tag{33}$$

Taking into account the equations shown in Formulas 32 and 33, a proper code is implemented in MATLAB, and the magnetic fluxes are calculated. For further detail, the implemented MATLAB code has been attached in Section 8.2 of the Appendix.

The fluxes obtained for the 230 V test and the 140 V test are of an amplitude of $3.66 \cdot 10^{-3}\ Wb$ and $2.22 \cdot 10^{-3}\ Wb$, respectively. These fluxes are divided by the cross section computed in Section 2.2.2, resulting into the peak magnetic density values of 1.58 T and 0.96 T.

Under rated operation, a value of 1.58 T is apparently reached. However, taking a look at the BH Curve provided by the manufacturer (Appendix Section 8.3) can be seen that this value still belongs to the linear region, while the highly distorted current in Figure 19, suggests that the transformer is operating already in the saturated region. Further analysis is made in order to solve this issue.

The measured current shown in Figure 19 has associated an intensity field H, as shown in Formula 34. By means of the manufacturer BH Curve, a magnetic density value of 1.87 T is obtained. The flux already computed by voltage integration, matches the B value obtained through the BH curve, only if a lower effective cross section is considered.

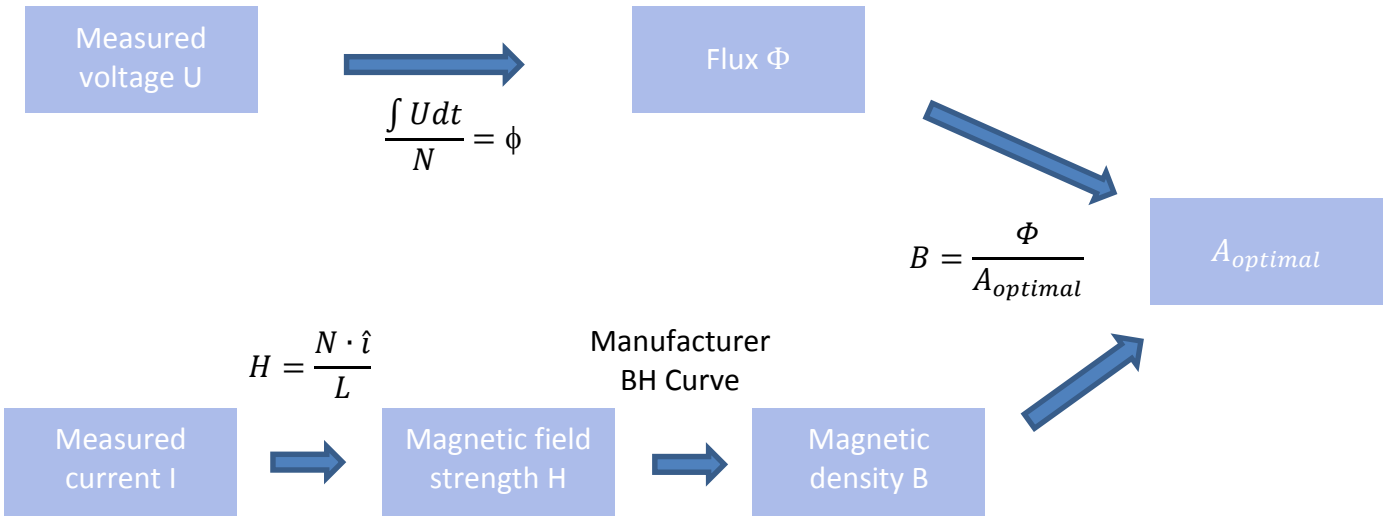

Figure 21: Process followed in the cross section computation

A sum up of the followed process is shown in Figure 21. However, the reader should be aware that several approximations were done throughout the computation of this section. The main path length shown in the already simplified equation used for computing the magnetic field strength H was calculated taking assumptions, as the data given by the manufacturer was not sufficient for obtaining the exact value. Taking this into account, it can be stated that exists certain variability in these calculations.

The effective cross section considered for rated voltage (230 V) and for lower voltage (140 V) are therefore

$$A_{optimal-230V} = \frac{\phi}{B} = \frac{3.66 \cdot 10^{-3}\ Wb}{1.87\ T} = 1957.2\ mm^2 \quad \textbf{(34)}$$

$$A_{optimal-140V} = \frac{\phi}{B} = \frac{2.22\ \cdot 10^{-3}\ Wb}{1.7\ \mathrm{T}} = 1305.8\ mm^2 \quad \textbf{(35)}$$

It can be noticed from these computations that, the lower the voltage applied to the transformer, the lower the value of the effective iron cross section is. A plausible explanation for this would be that when flux gets lower, as a consequence of supplying the transformer with a lower voltage, the resistance that shows the iron core to the flowing flux, i.e. the reluctance, could make that the flux lines focus on a narrower section, not being uniformly distributed all over the cross section. It is remarkable to say that the flux lines always tend to flow through the shortest path, so that the total reluctance is the lowest.

As a consequence of this, the effective cross section would be dependent on the magnitude of this flux, and, therefore, on the voltage supplied. In Chapter 5 the model simulations are presented and will help with the verification of this matter.

Once that the magnetic flux density B and the magnetic field strength H are computed, the hysteresis curves are plotted in Figure 22 and Figure 23.

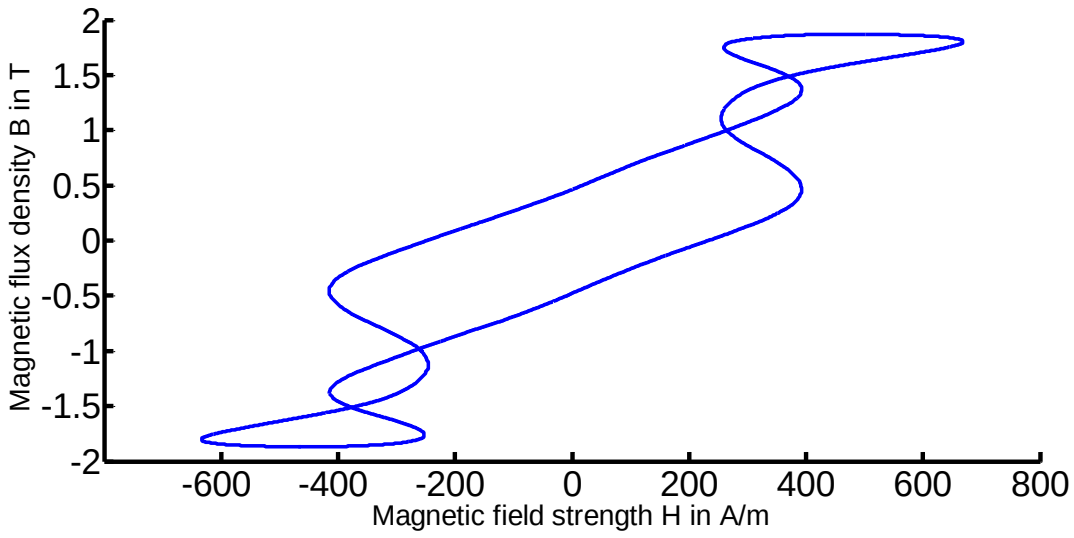

Figure 22: BH Curve for a 230 V hysteresis test

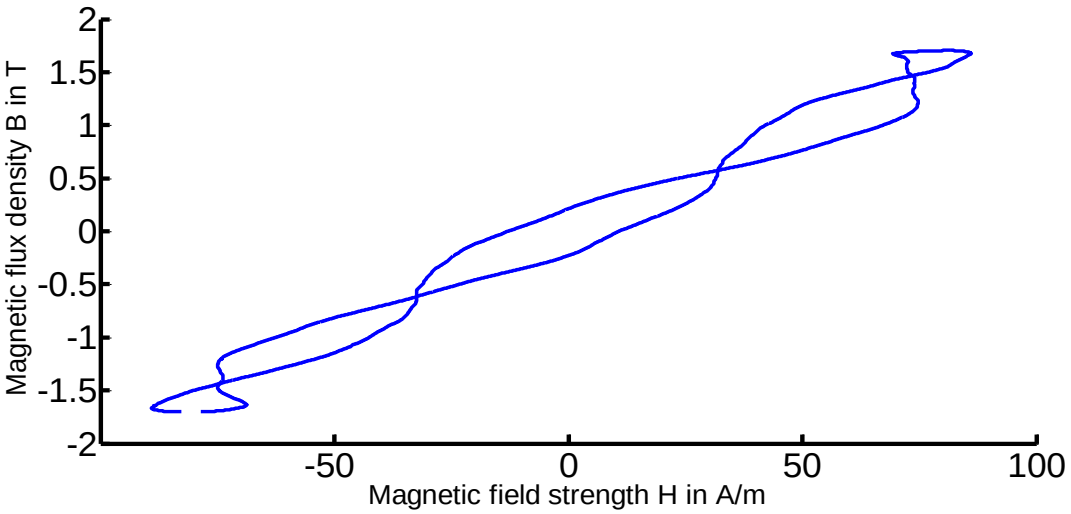

Figure 23: BH Curve for a 140 V hysteresis test

The expected plot of a BH Curve would be far from the one obtained in the figures above. A strong interaction between phases is suspected to be the fact that leads to the observed results. Therefore, further analysis must be made in order to understand how this interaction exactly is.

4 Transformer parameters implementation

The main goal of the measurements shown in Chapter 3 was to obtain as closely as possible the real parameters of the transformer, so that reliable simulations can be carried out.

In Table 5, the different parameters implemented into the MATLAB model are shown.

Table 5: Parameters implemented in the MATLAB model

Rated Power	$2\ kVA$
Phase voltage V_1	$231\ V$
Number of primary turns N_1	277
Number of secondary turns N_2	286
Phase voltage V_2	$231\ V \cdot \frac{286}{277} = 238\ V$
Frequency	$50\ Hz$
Rated primary current I_{1N}	$2.98\ A$
Rated secondary current I_{2N}	$2.89\ A$
Resistance of primary side winding R_1	$0.844\ \Omega$
Resistance of secondary side winding R_2	$1.125\ \Omega$
Power losses in iron P_o	$26.81\ W$
Short-circuited voltage $u_{k\ av}$	0.0085
Average length of limbs L_i	$173.28\ mm$
Average length of yokes Y_i	$60\ mm$
Effective section of limbs and yokes $A_{Li,Yi}$ for rated conditions	$1957.2\ mm^2$
Weight of core limbs	$3.181\ kg$
Weight of yokes	$1.101\ kg$

B-H Characteristic of Iron Core	Look-up Table

A sum-up of the way each parameter is obtained is shown below in Table 6.

Table 6: Relation between the different model parameters and their origin

Rated Power, frequency, phase voltages and number of turns	taken from the **m**anufacturer data.
Winding resistances	set according to Section 3.1.
Short-circuited voltage $u_{k\,av}$	introduced according to the value computed in Section 3.3.
Average length, section and weight of core limbs and yokes	introduced as shown in Section 2.2 according to the core geometry data supplied by the manufacturer and the iron core properties.
B-H Characteristic of Iron Core	implemented through a look-up table composed of ten points, taken out from the iron manufacturer curve. Both the manufacturer curve and the discretized one can be found in Section 8.3 and 8.4 of the Appendix, respectively.
Real power losses in the iron	approximately equal to the total power losses in rated conditions (given by the manufacturer) minus the copper losses due to the resistances of the windings. This is successfully corroborate with the no-load test power lecture shown in Section 3.2.

5 Comparison between real measurements and model simulations

One of the main goals of this thesis, highlighted at the beginning of the work, is the verification of the MATLAB model with the laboratory measurements. Therefore, special dedication has been employed in this chapter towards this purpose, where several comparisons regarding the behavior of the model and the real transformer are shown.

The scenarios chosen for these comparisons comprise:

- No load test
- Short Circuit test
- Hysteresis test
- DC Analysis

5.1 No-load test

In section 3.2, several no-load tests with different voltages were carried out. In order to verify our model in a wider way, comparisons within a voltage range between 70 V and 230 V were done.

As a first step, the iron cross section computed in Section 2.2.2 through the effective cross section factor given by the manufacturer is introduced in the model. As expected, the results does not seem to match in an acceptable way the real measurements. Therefore, the section is adjusted following the process shown in Section 3.4. Since it exists variability in the computations of it, the optimal section for the model could be within an interval margin. The effective cross section of the iron used in the simulations is 1957 mm^2.

Another important consideration is the asymmetrical lecture of the iron losses read during the measurements. Each phase contributes differently to the total sum, as shows Table 7.

Table 7: 230 V no-load test results

Average Power of phase R	9.55 W
Average Power of phase S	3.87 W
Average Power of phase T	12.88 W
Total sum	26.30 W

In the electric circuit of the model, these losses are represented through a resistance (R_{mA}), as illustrates Figure 24.

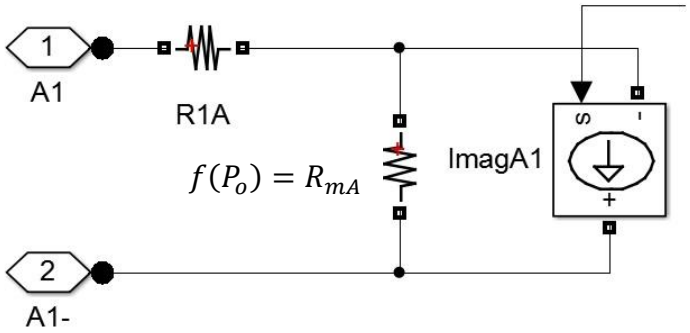

Figure 24: Electrical modelling of the iron losses

These resistances are for all phases equal in the model since they are computed as a function of the total iron losses P_o for rated conditions, and do not take into account the contribution of each phase. The resistance and the power losses show a linear relation, as shows Formula 36.

$$R_m \propto \frac{U_{nom}{}^2}{P_o} \tag{36}$$

The bigger the iron losses in one phase, the smaller the resistance, and, since the voltage remains constant, the higher is the electrical current associated to this losses.

This limitation affects in some scenarios negatively to the simulation results. Therefore, taking into account the contribution of each phase to the total iron loss shown in the previous table, and modifying the value of each resistance, more accurate results can be obtained.

The measured data and the simulations were overlapped in one graph, for a better visualization.

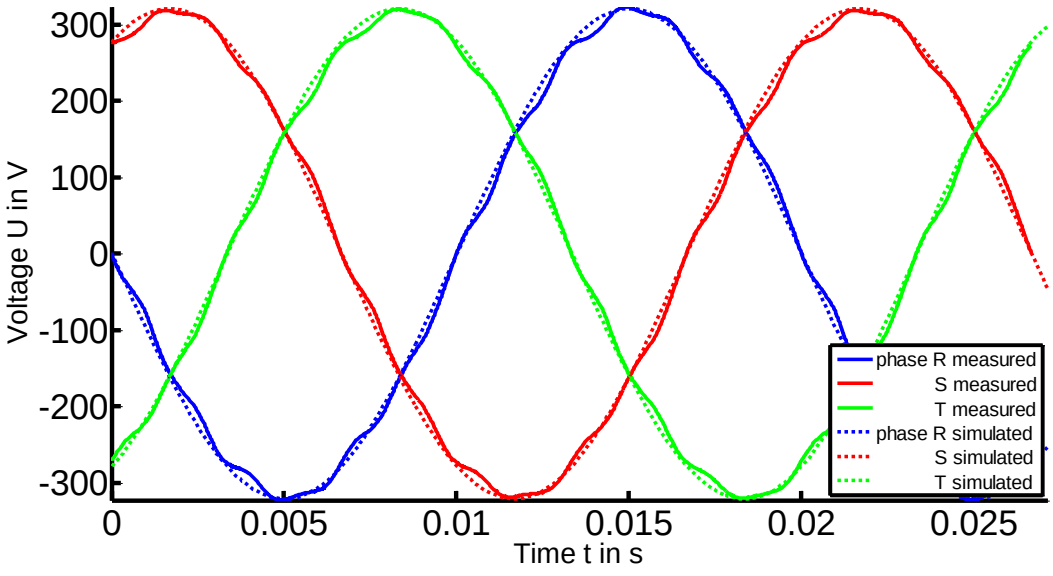

Figure 25: Voltages comparison in a 230 V no-load test

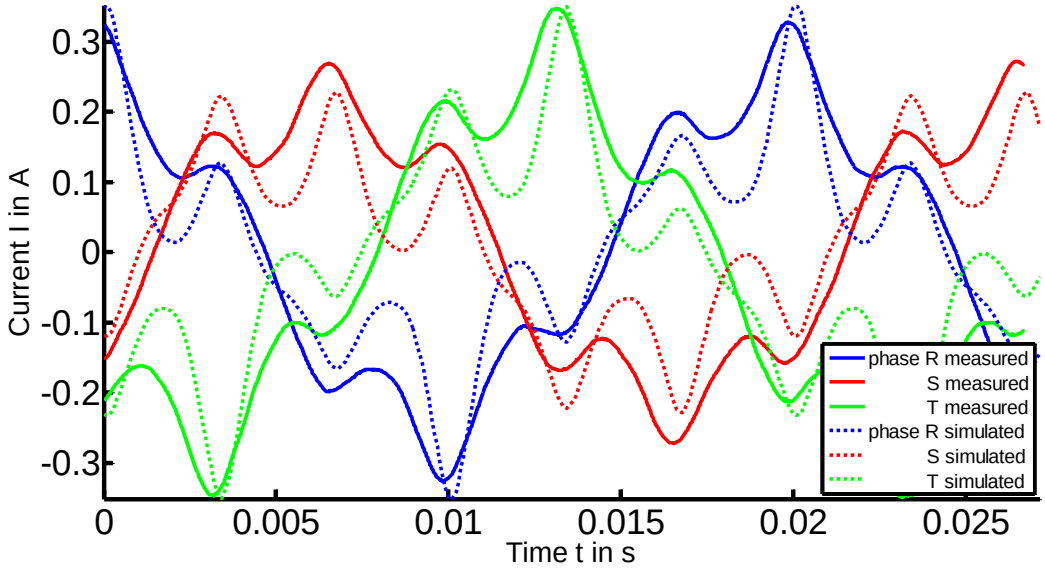

Figure 26: Currents comparison in a 230 V no-load test

Regarding the 230 V comparison shown in Figure 25 and Figure 26, an appreciable discrepancy between the measured currents and the simulated ones can be seen at the saturation peaks of each phase. The extra current that one phase need during its saturation, is delivered by the other two phases, resulting into a deviation from what would be a non-saturated sinusoidal line. In the simulation these deviations are more emphasized, whereas in the real transformer are softer, and smaller in amplitude.

In Figure 26 can also be seen that the phase-shift between phases in the measured currents and the simulated ones is not exactly the same. The different behavior between model and the real transformer could be explained through the concept of mutual inductances between phases. Several construction differences, i.e. the numbers of turns, the disposition of the three windings along the iron core and the geometry, enhance these asymmetries between phases [2]. However, the model used in the simulations does not take into account these mutual inductances, which determine how the interaction that occurs between phases is. This is considered as a limitation of the model and is left to further investigation.

Another remarkable consideration to take into account is the unbalanced voltage supply provided by the step-up transformer. In some cases, the voltage difference between phases was observed to be up to 9 V. However, in the model, the simulations were carried out with perfect balanced voltage supply.

An expected phenomenon occurs when the voltage supply is set lower. As can be seen in Figure 27, the model does not seem to adjust well in this scenario. While the real transformer

is still in the saturation region, the model seems to be in a more linear one, as the currents are rather more sinusoidal and lower in amplitude.

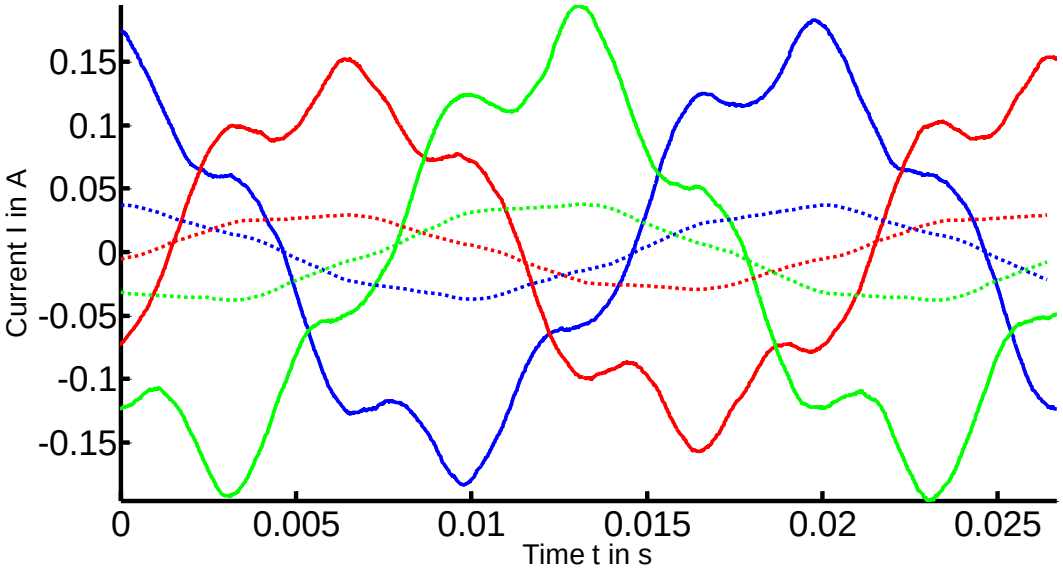

Figure 27: Currents comparison in a 200 V no-load test

In accordance to the explanation mentioned in Section 3.4, the effective cross section introduced in the model was reduced to $1795\ mm^2$ for the 200 V supply test, and the results improved significantly, as can be seen in Figure 28.

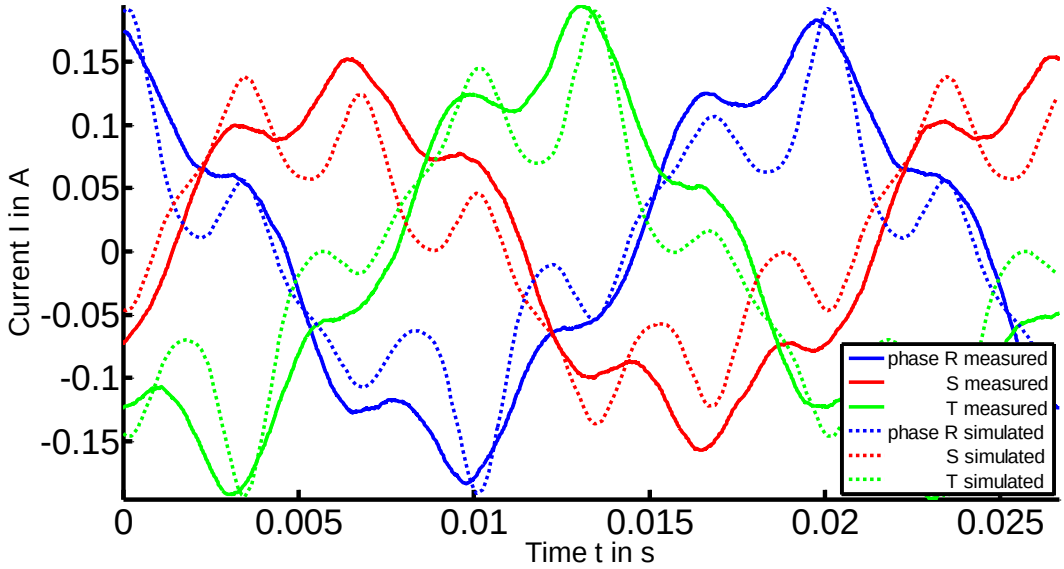

Figure 28: Currents comparison in a 200 V no-load test (II)

As the voltage supply keeps dropping down, the transformer gets out of the saturation region to reach a more linear one, where the magnetization curve is such that, variations on the density flux B imply very small variations on the magnetic field strength H, and therefore, on the excitation currents. Due to this fact, the model response for this range of voltages remains

unchanged for variations on the cross section. This fact can be observed in the manufacturer BH curve, attached in Section 8.3 of the Appendix.

Another no-load test comparison with a lower voltage is shown in Figure 29 and Figure 30.

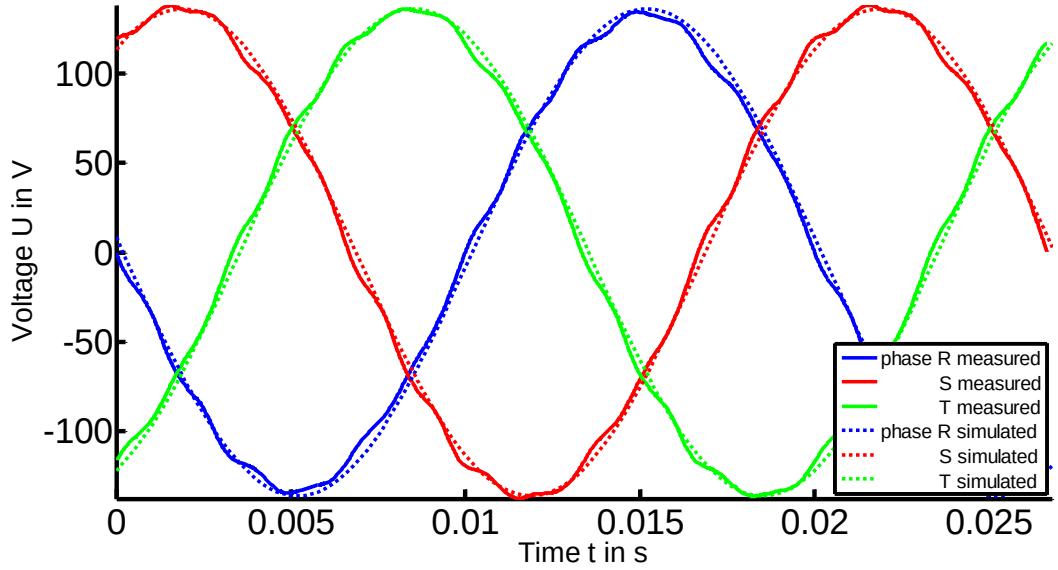

Figure 29: Voltages comparison in a 100 V no-load test

As can be seen in Figure 30, the model adjusts well to the transformer real behavior. However, an appreciable noise and a phase shift that did not exist before can be appreciated. As men-

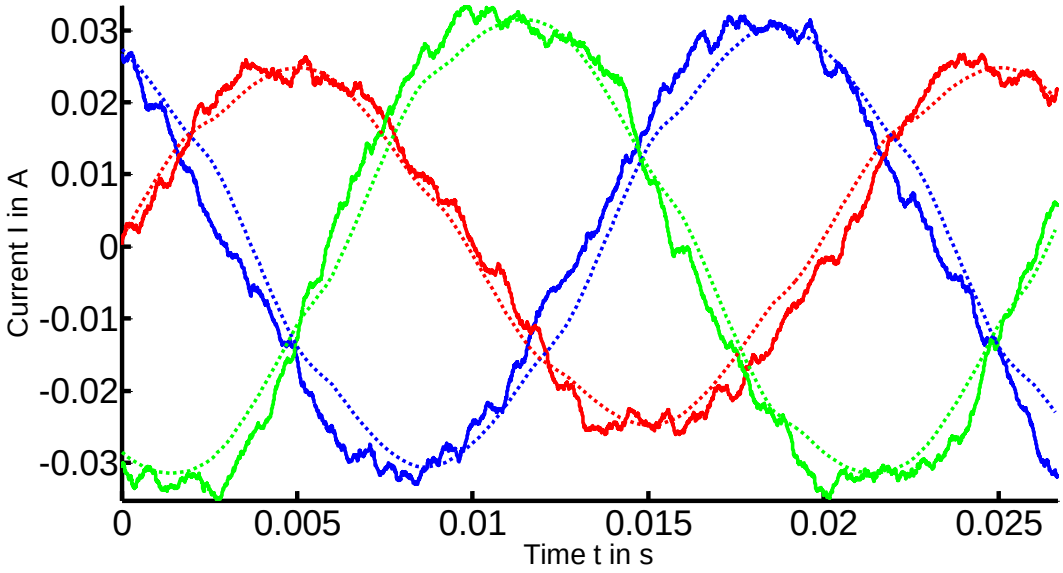

Figure 30: Currents comparison in a 100 V no-load test

tioned before, for small output voltages, the step-up transformer supplies a more unbalanced

and distorted voltage. Besides this, the current clamp used in the measurements is accurate in the range of 25 mA – 20 A, so in this situation it is operating close to its lower limit.

Regarding the iron losses, a comparison between the model and the power lectures of the real transformer is shown in Figure 31, for different voltages.

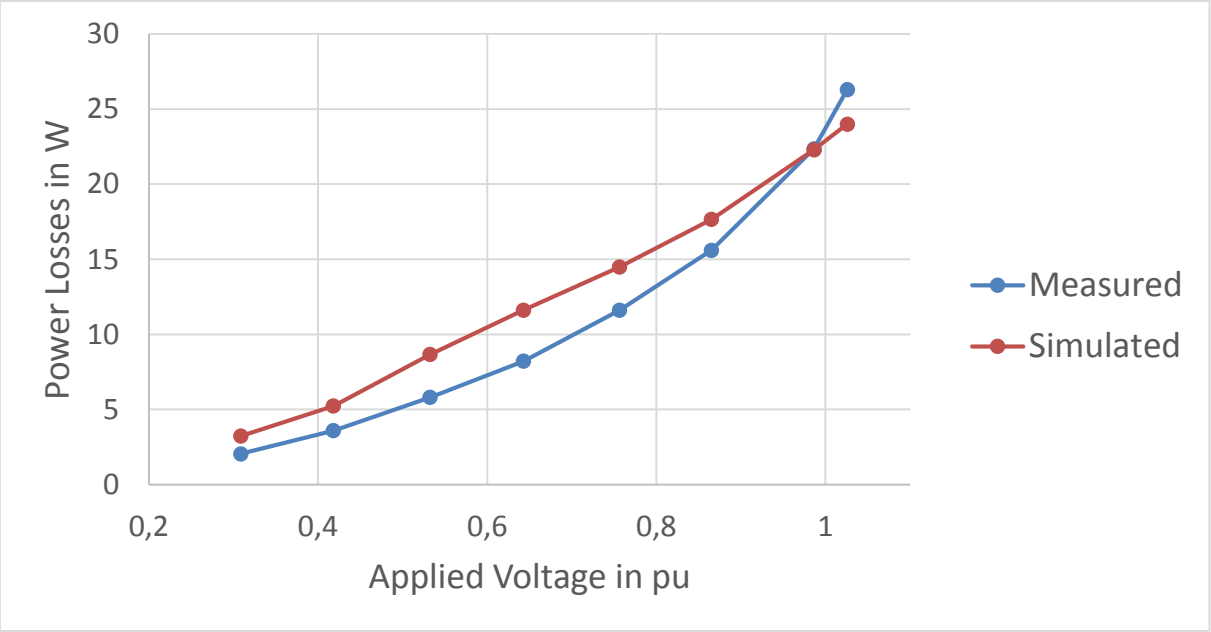

Figure 31: Power consumption comparison for different applied voltages

As explained in the description of the model at the beginning of this work, the model computes the iron losses taking the flux density value B, and multiplying the associated loss provided by the manufacturer in the B-P Curve, by the mass of the corresponding segment. As the voltage drops down, a lower value is introduced for the effective iron cross section. Therefore, the mass of the iron core involved in the power losses computations is reduced too, according to Formula 37.

$$mass = density \cdot volume\ of\ each\ segment = \rho \cdot L \cdot A_{eff} \quad (37)$$

As the model does not take into account the different asymmetries of the real transformer in order to compute the iron losses, an equal value can be read in each phase. The model show slightly greater power losses than the real ones for voltages under 230 V, and a more linear behavior.

5.2 Short-circuit test

The value obtained from the short-circuit test in Section 3.2 is introduced in the model, and a simulation is carried out, obtaining the dotted waveforms shown in Figure 32 and Figure 33.

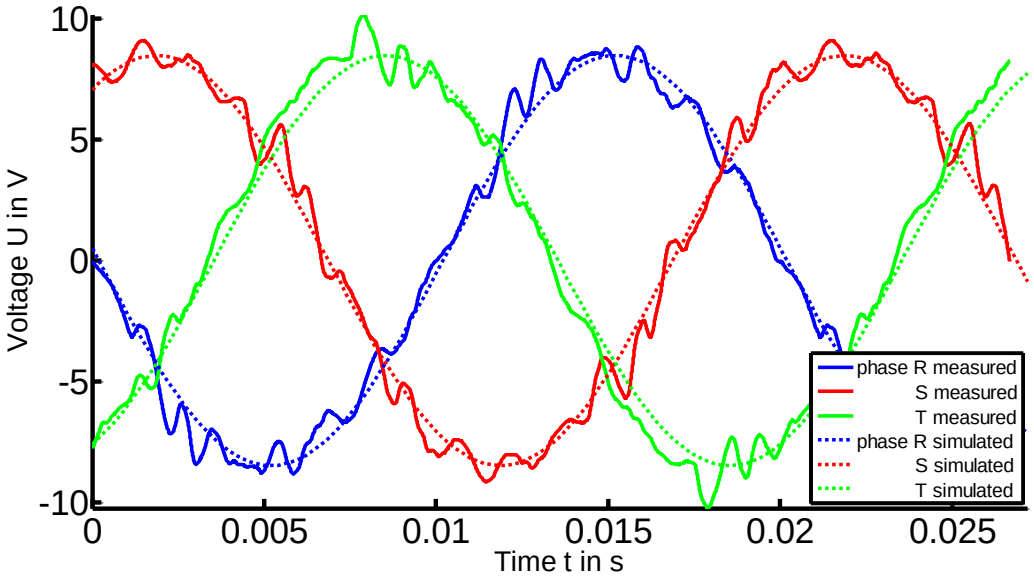

Figure 32: Primary voltages comparison in a short-circuit test

As mentioned in Section 3.3, due to the low voltages required in this test, the feeding transformer provides an unbalanced and distorted voltage supply. However, the model simulation adjusts well to the real measurements.

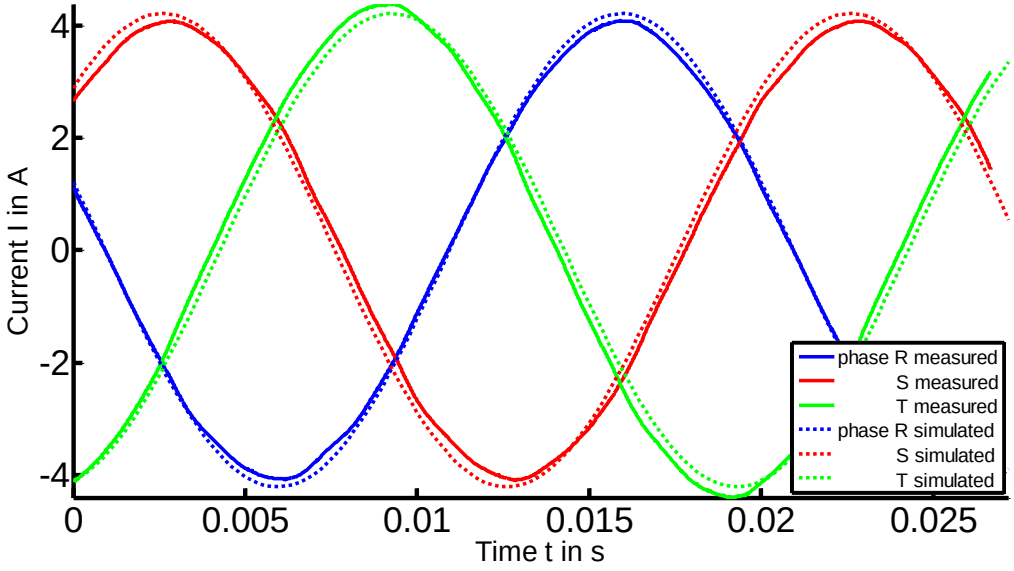

Figure 33: Currents comparison in a short-circuit test

5.3 Hysteresis test

In Figure 34 and Figure 35, the computed fluxes from the measurements (230 V and 140 V) are compared with the ones simulated on the model. As can be observed, very close results are obtained.

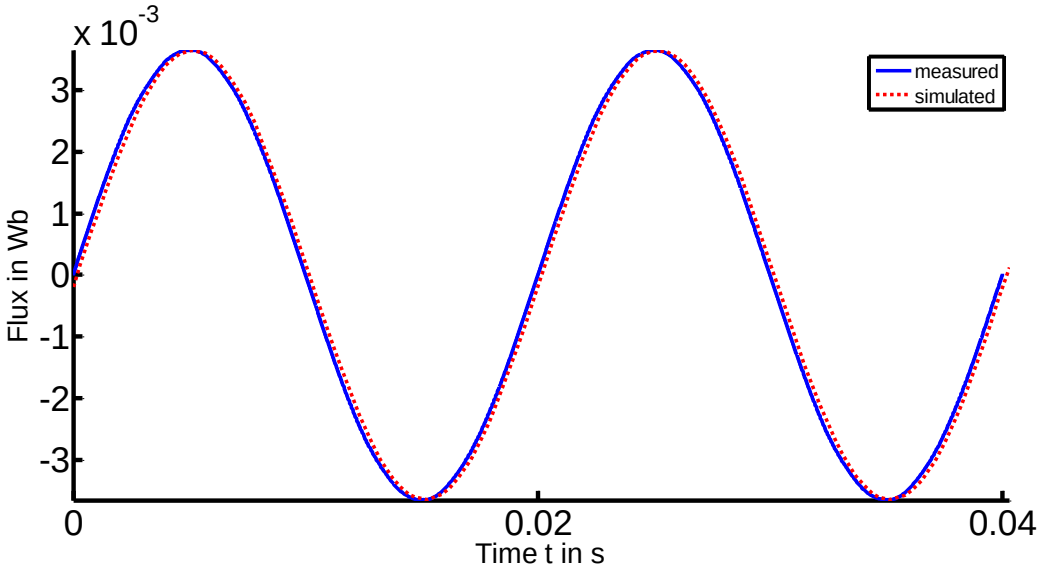

Figure 34: Fluxes comparison in a 230 V hysteresis test

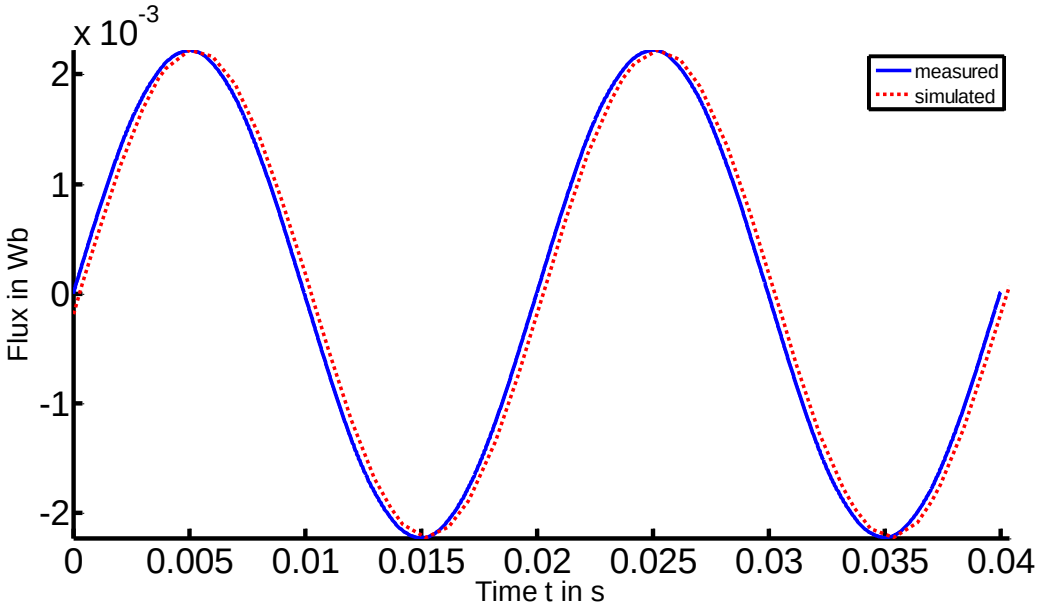

Figure 35: Fluxes comparison in a 140 V hysteresis test

6 DC Analysis

After having measured the main parameters of the transformer, and having seen the behavior of the real transformer and the model under different scenarios, an analysis of the behavior of the transformer under DC component is presented in this chapter.

For that purpose, the scenario shown in Figure 36 is chosen for the measurement series. In this scenario, two identical transformers are connected back-to-back, from the secondary of the first transformer (Transformer 1) to the secondary of the second (Transformer 2), through a 1 Ohm resistance per phase. The DC current is injected then by means of a DC current source set between the secondary neutral terminal of Transformer 1 and the secondary neutral terminal of Transformer 2. This second transformer works with no load.

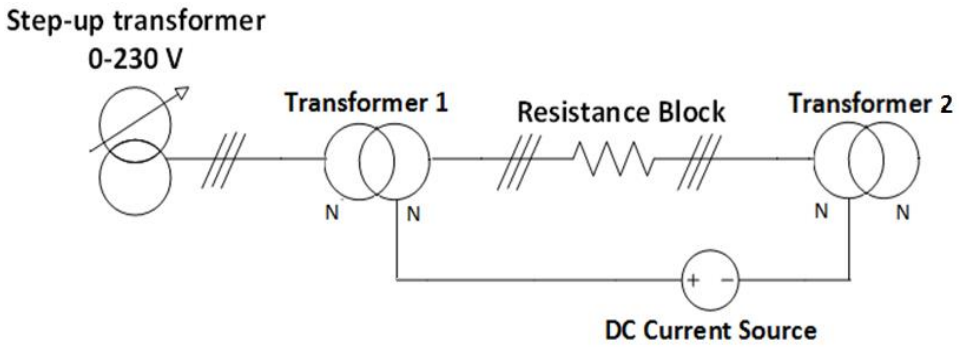

Figure 36: DC Setup used in the measurements

The DC current flowing through the neutral points of both transformers induces an offset on the fluxes flowing inside the iron core, as shown in Figure 37 [5].

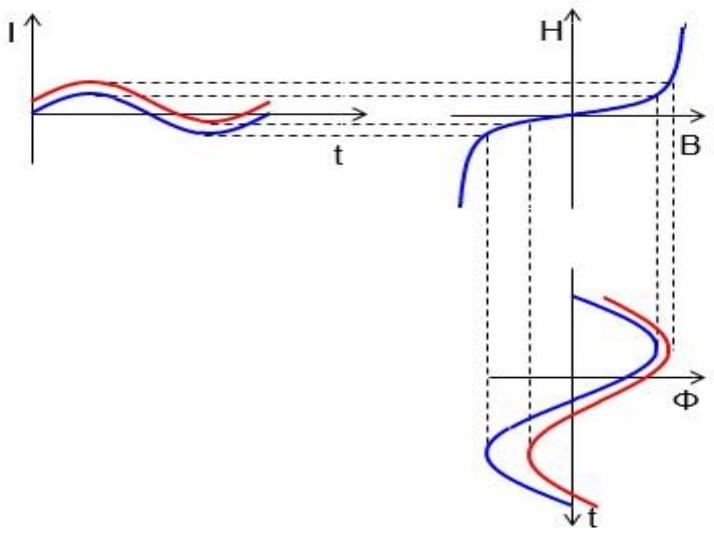

Figure 37: Generic biased current related to a biased flux

The greater the DC injection, the greater the induced offset is. The shifted current flowing now through the windings implies also a shift on the working region of the BH Curve. Therefore, the magnetic flux shows also an offset.

In the first scenario, dealt in Section 6.1, the same amount of DC is desired to be introduced in each of the three phases, creating a symmetrical case. In the second scenario, an unbalanced situation is induced.

The DC analysis was carried out in first place under rated conditions. The effects due to DC on the transformer behavior was not as clearly appreciated as expected. As can be seen in the generic BH Curve shown in Figure 38, the transformer is under these circumstances already saturated, and the effect of the DC was partially hidden.

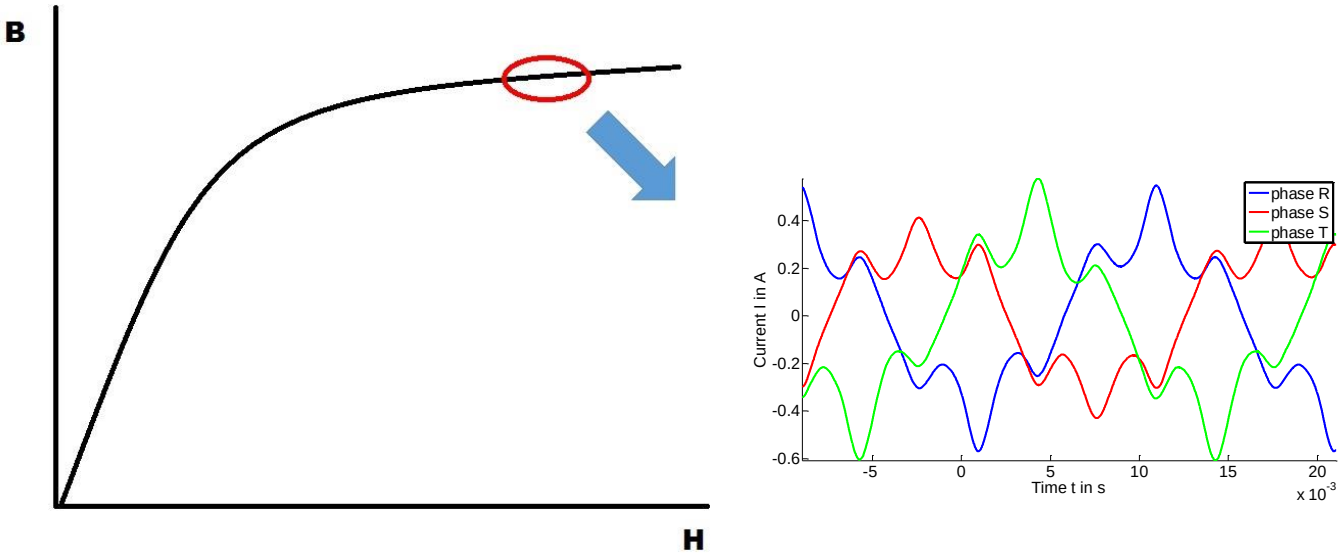

Figure 38: Maximum point reached in the BH Curve and associated currents

In order to appreciate better the effects caused by the DC current injection, a lower voltage is supplied to the setup, so that the transformer works out of the saturation region, as shown in Figure 39.

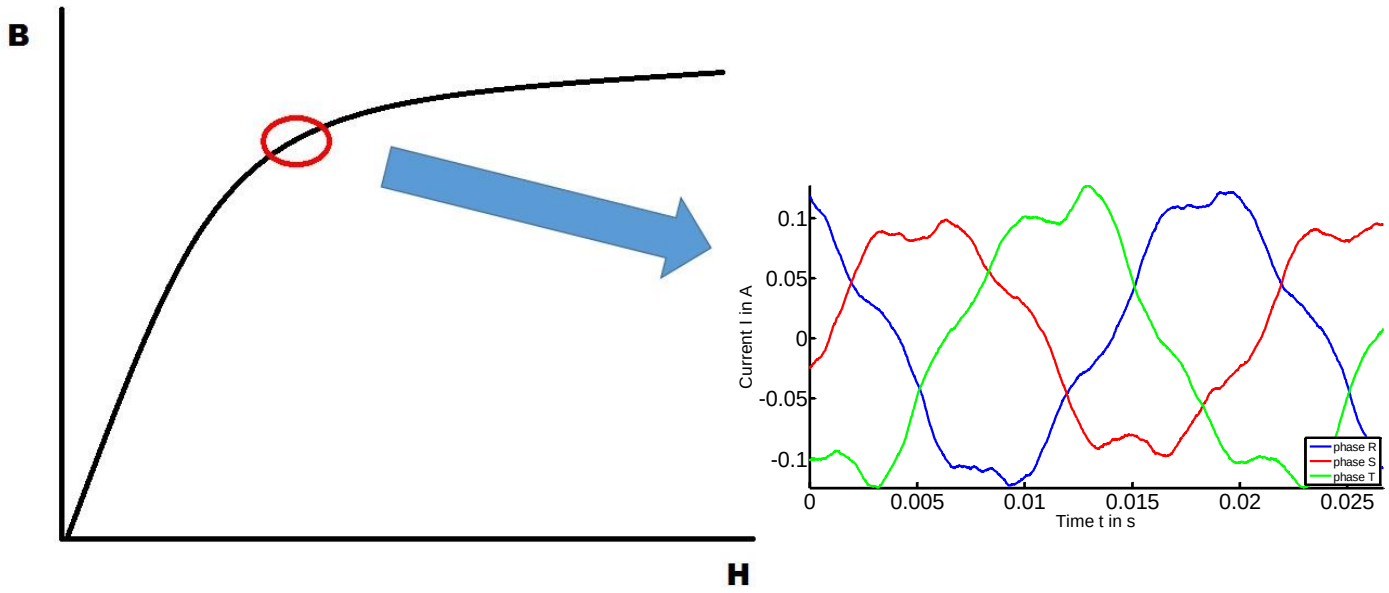

Figure 39: Maximum point reached in the BH Curve and associated currents (II)

6.1 Balanced DC current injection

In this scenario, both transformers are connected to each other directly, with no resistances between them, in order to induce equal DC current in each phase.

Having a look into Figure 37 it can be seen that, since the excitation current has now an offset, so it has the magnetic field strength. The working region on the BH Curve has been therefore shifted, and consequently, the magnetic flux.

Regarding the flux distribution over the structure of the iron core, both situations, with and without DC offset are shown in Figure 40 [5]. If it is considered, for example, the precise moment where the alternating flux flowing through the central phase reaches its maximum value, the situation is the one shown in the figure.

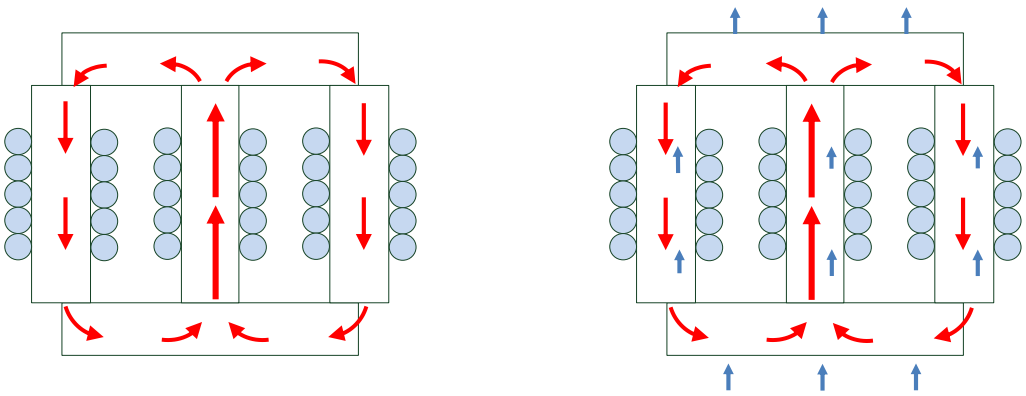

Figure 40: Magnetic flux distribution without DC offset and with symmetric DC offset (blue arrows)

When a DC component is introduced, the magnetic flux is then composed by a sinusoidal flux component (red arrows) and a DC component (blue arrows). The sinusoidal component is distributed in the iron core in the same way than it did with no DC, whereas the DC component must close its path getting out from the iron core through the air or tank, when exist. This path outside the iron core has a significantly higher magnetic reluctance, and therefore, high DC currents are required in order to get a significant DC flux component.

In the following graphs, the peak value of the primary AC currents of the transformer connected to the power supply (Transformer 1), is plotted against the DC injected current. Besides this, an analysis of the power increase with the DC injection was also considered of high interest, and therefore several plots have been made towards this purpose. All the values are in pu, and are referred to the values measured without DC, as shows Formula 38.

$$\frac{i_{AC\ under\ DC}}{i_{AC\ under\ no\ DC}} = f(i_{dc}) \tag{38}$$

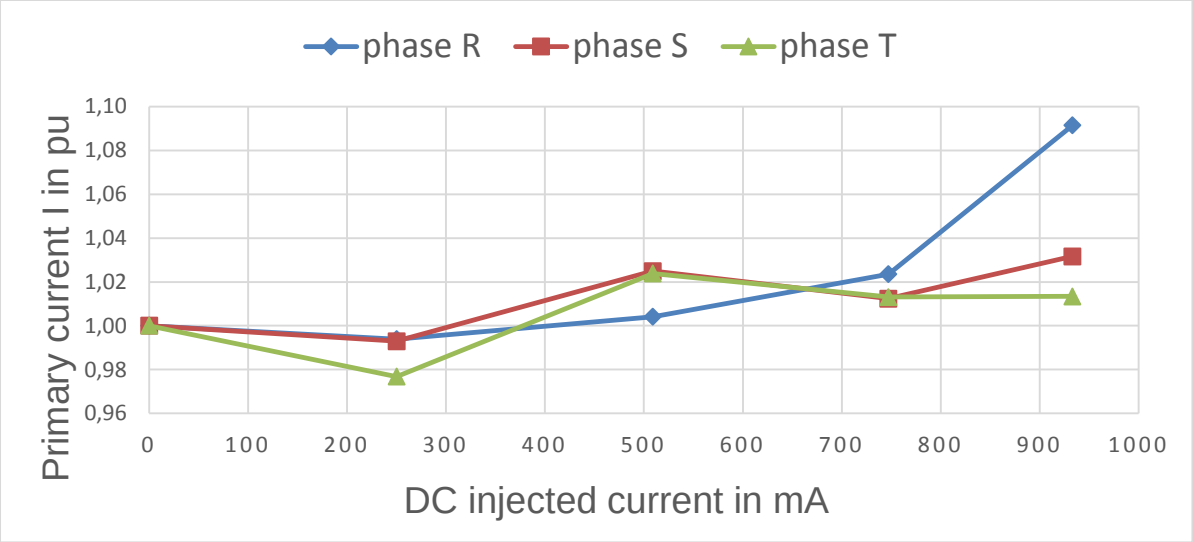

Figure 41: Maximum value of the primary currents of Transformer 1 with DC current injection

As can be seen in Figure 41, the injection of different levels of DC in the setup seems to have no big effect on the peak values of the current. The real power consumption of the whole setup shows a slightly increase, as can be seen in Figure 42. This one is, however, irregular and not significant, as the transformer does not get into an appreciable level of saturation. It must be noticed that, as the DC component has been removed, all the computed powers belong to AC components.

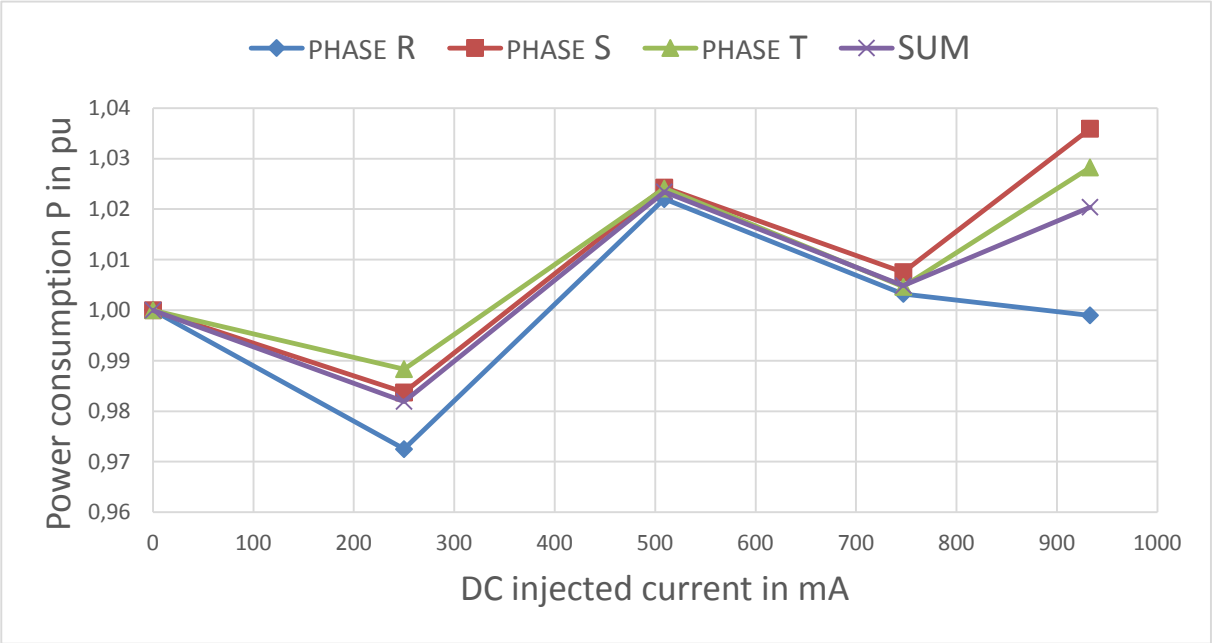

Figure 42: Power consumption of Transformer 1 with DC current injection

Same trend is observed when Transformer 2 is analyzed. It is remarkable to say, that Transformer 1 currents are for all DC injections, double than currents in Transformer 2. This corresponds to the fact that the first transformer demands the current necessary to magnetize itself and also the second transformer, which is identical. Concerning the real power consumption, the same situation is found: Transformer 1 power consumption is for all DC injection between 2 and 3 times the one of Transformer 2. Furthermore, the apparent power S that demands the whole setup is computed for different levels of DC, and no significant effects are observed.

An interesting effect that the DC injection produces on the output phase-to-ground voltage of Transformer 1 can be seen in Figure 43.

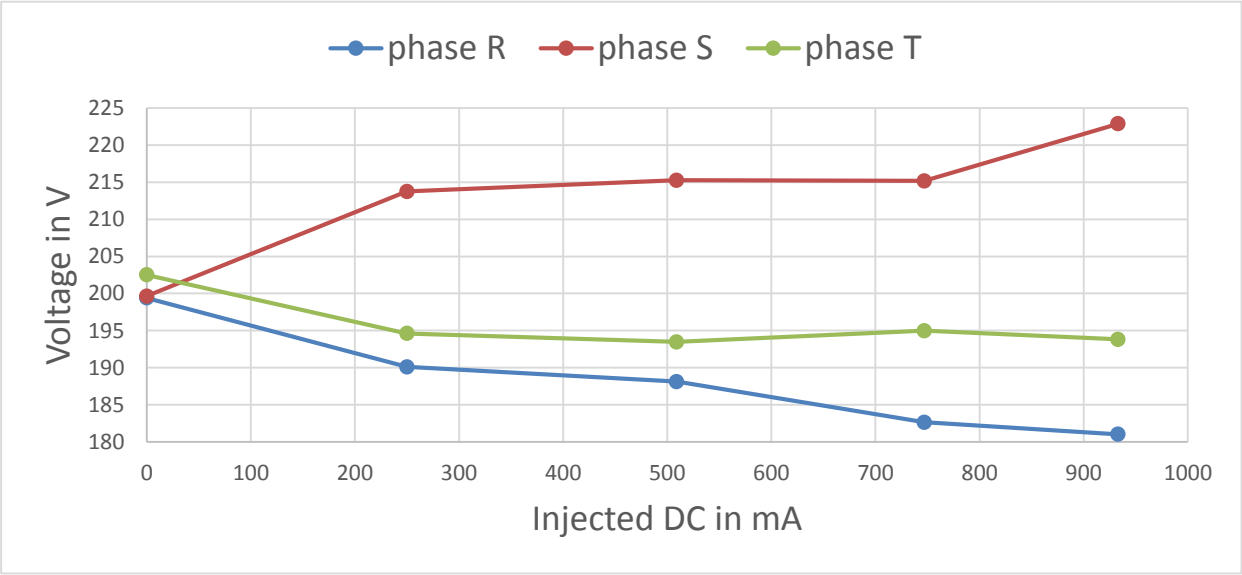

Figure 43: Voltage supplied by Transformer 1 to Transformer 2 under balanced DC injection

Phase S shows an increasing tendency of its voltage as the DC injection grows. On the other hand, the external phases, R and T show a decreasing tendency instead. This phenomenon of getting an unbalanced secondary voltage due to DC current injection can be also found in previous works among the consulted literature [7].

Except for this last effect, it can be said that under symmetric DC injection, the setup composed of the two transformer reflects no big change compared to the situation when no DC is applied. The excitation currents as well as the real and apparent power values do not show great variation. Previous works regarding DC injection on power transformers, also reflect this fact [5].

6.2 Unbalanced DC current injection

An unbalanced DC current is now injected through each of the three phases, by means of 1 Ω resistances set between both transformers. The resistances are set in two of the three phases, whereas no resistance is connected to the phase where the unbalanced current is desired to flow.

The greater magnetic flux offset that now flows through the limb of the unbalanced phase has to close its path. The available paths with the lowest reluctances are now the two limbs of the other phases, specially the central limb of phase S, which has the shorter path and therefore, the lowest reluctance. An example of this scenario is represented in

Figure 44, where is considered the precise moment when the sinusoidal flux flowing through the central phase reach its maximum, and a greater unbalanced DC current is injected on it.

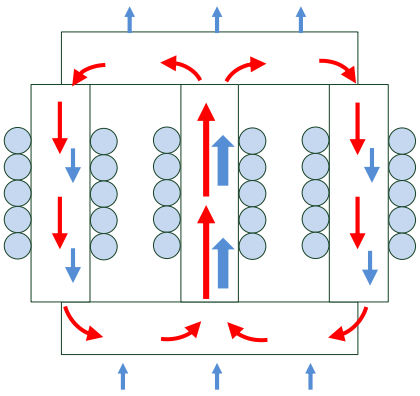

Figure 44: Magnetic flux distribution with unsymmetrical DC offset (blue arrows)

It is important to notice that, due to the available lower-reluctance paths, greater flux offsets compared to the symmetrical case are achieved.

As done in the previous section, the variations observed in Transformer 1 currents are firstly graphed for the different unbalanced scenarios. These graphs are shown from Figure 45 to Figure 47.

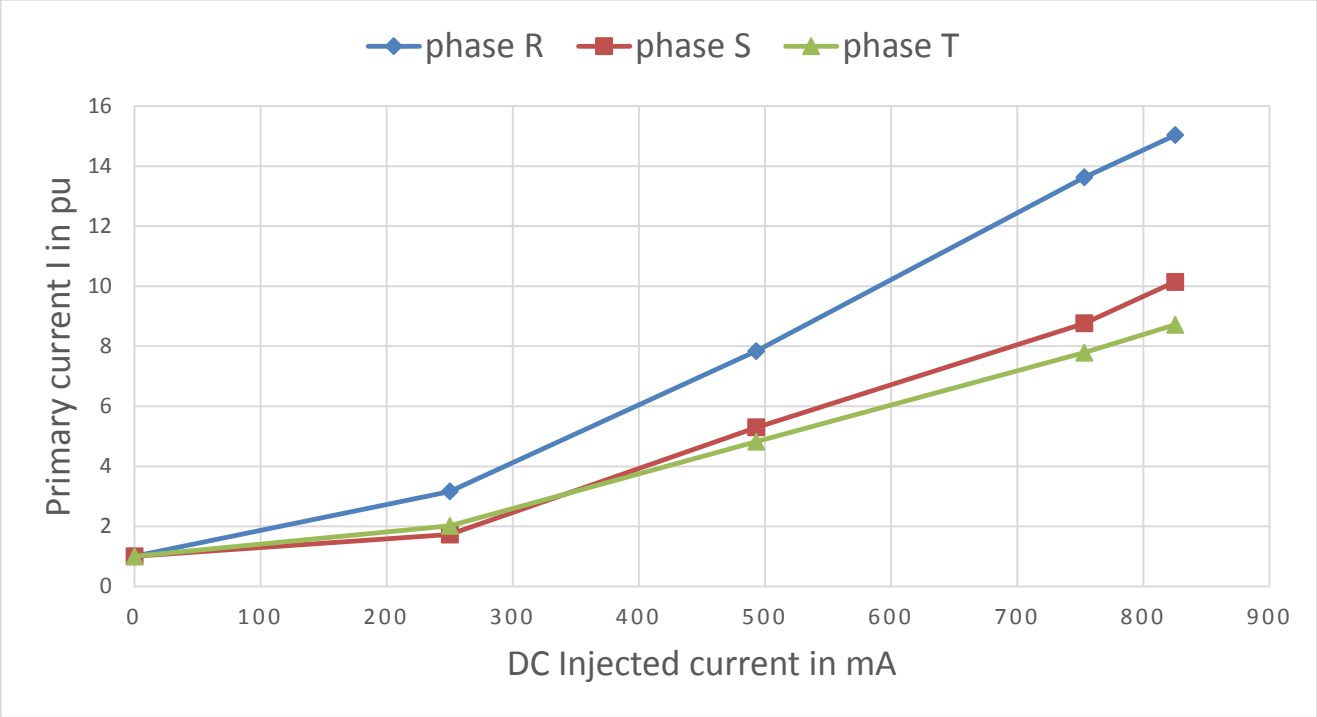

Figure 45: Variations of the primary current of Transformer 1 with DC Bias when no resistance is set in phase R

Appreciable differences compared to the balanced case can be observed at first glance. Having a look at Figure 45, it can be seen that for low DC injection, the unbalanced phase demands a magnetizing current of 3 times the value without DC, and on the other phases, twice the current that is demanded without DC.

For medium and higher DC injection, a major rising rate can be observed in the plots: the magnetizing current increases its value with a bigger rate. When high level of DC is injected, a value of 15 times the value without DC injection is achieved on the unbalanced phase, and a value of approximately 9-10 times the value without DC is reached on the other phases. The transformers get into a higher level of saturation as the DC increase.

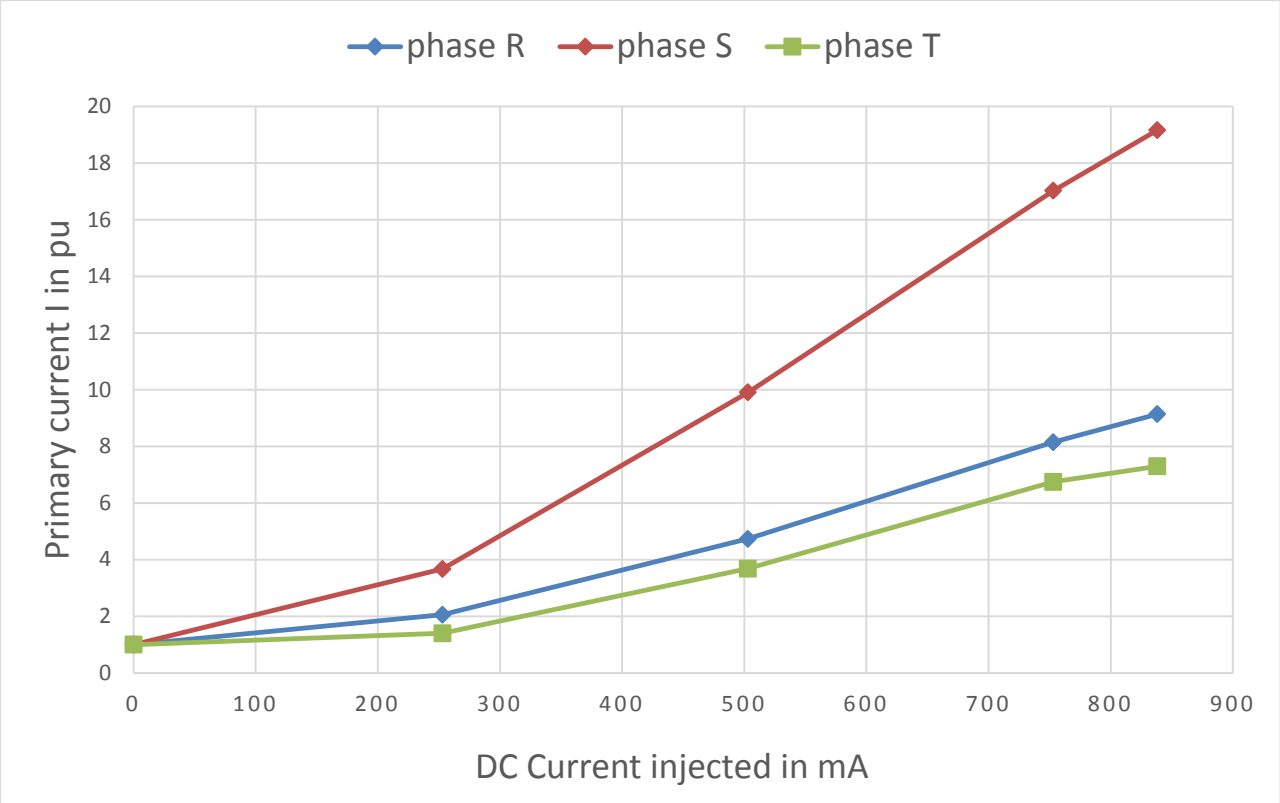

Figure 46: Variations of the primary current of Transformer 1 with DC Bias when no resistance is set in phase S

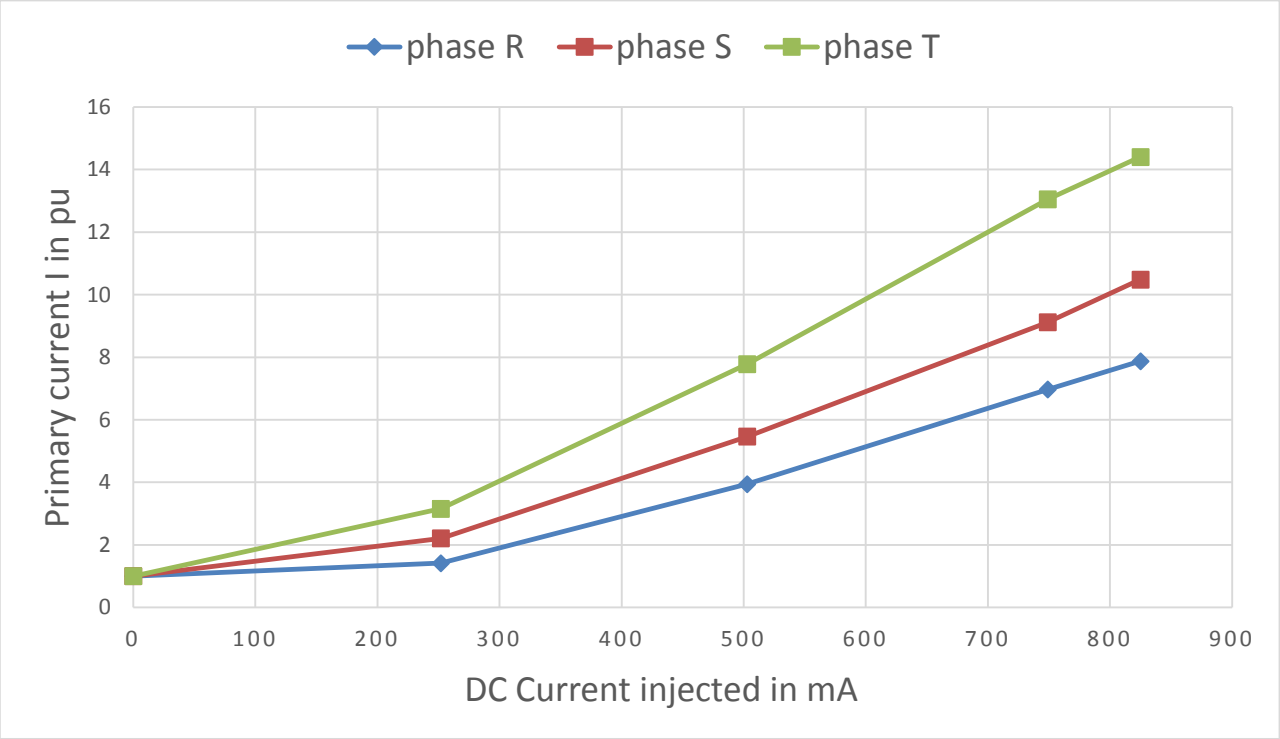

Figure 47: Variations of the primary current of Transformer 1 with DC Bias when no resistance is set in phase T

The reader can notice that the same trend is present in the other phases. In Figure 46, where phase S is the phase with the unbalanced current, a 19 times bigger current is observed for high DC injection, which is a greater value than the ones achieved in the unbalanced cases of

the external phases. However, it must be taken into account that phase S always demands a lower magnetizing current, as has been seen several times along this thesis, due to its lower reluctance. Therefore, a bigger effect of the DC current on this phase can be expected.

The currents observed in Transformer 2, follow a very similar trend to the ones observed in Transformer 1, and the maximum pu values achieved by the unbalanced phases are of 27 for phase R and phase T and 36 for phase S. Once again when the unbalanced case is induced for phase S, the maximum value of the current is found.

As happened in the symmetrical case, when the DC current is injected, an increasing tendency of the phase-to-ground output voltage of phase S of Transformer 1 is also observed, whereas a decreasing tendency is also observed in the other phases. As can be seen in Figure 48, a value of approximately 25 V difference can be observed for no DC injection, due only to the different AC currents flowing through the phases, and a value of 42 V difference for high levels of DC.

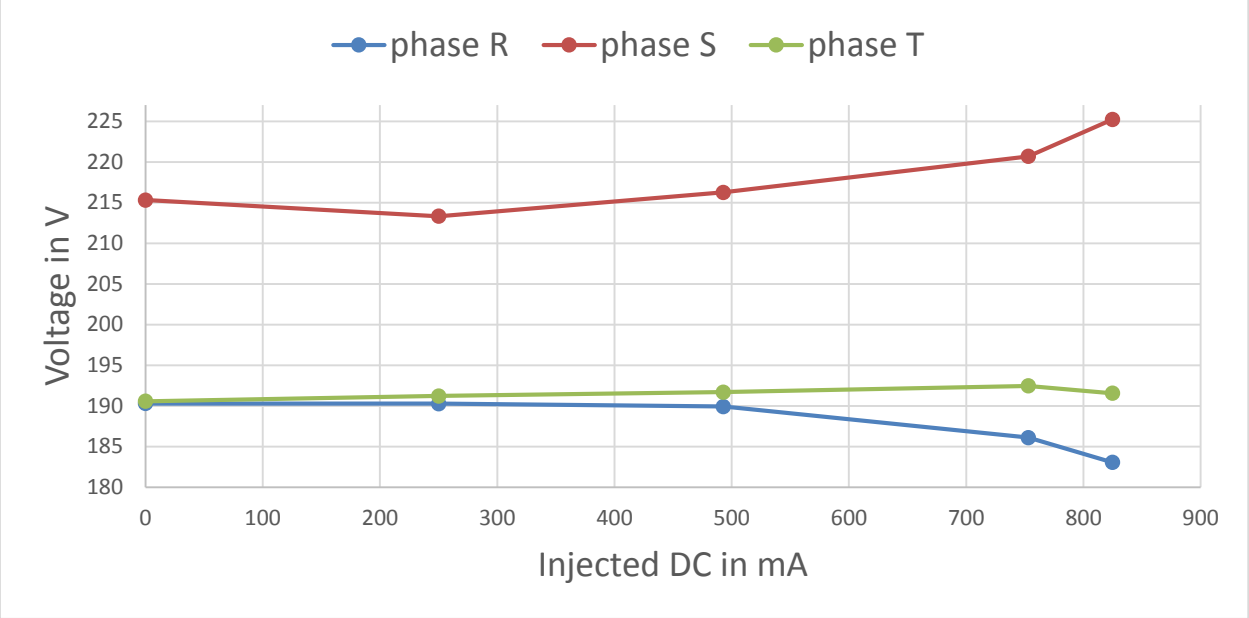

Figure 48: Voltage supplied by Transformer 1 to Transformer 2 under unbalanced DC injection

Concerning the real power consumption, the results are shown in Figure 49-Figure 51. The pu values are referred to the value of the power when no DC is injected.

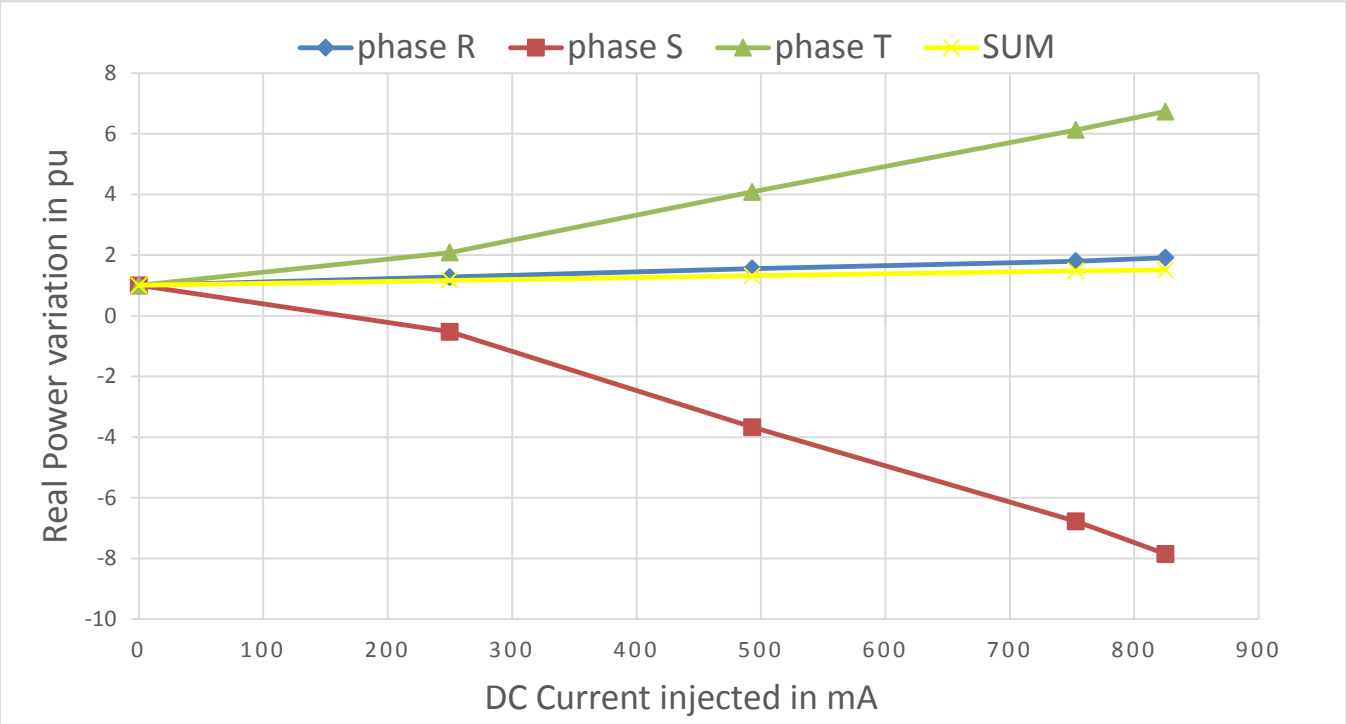

Figure 49: Real power consumption in Transformer 1 against DC current injection when no resistance is set in phase R

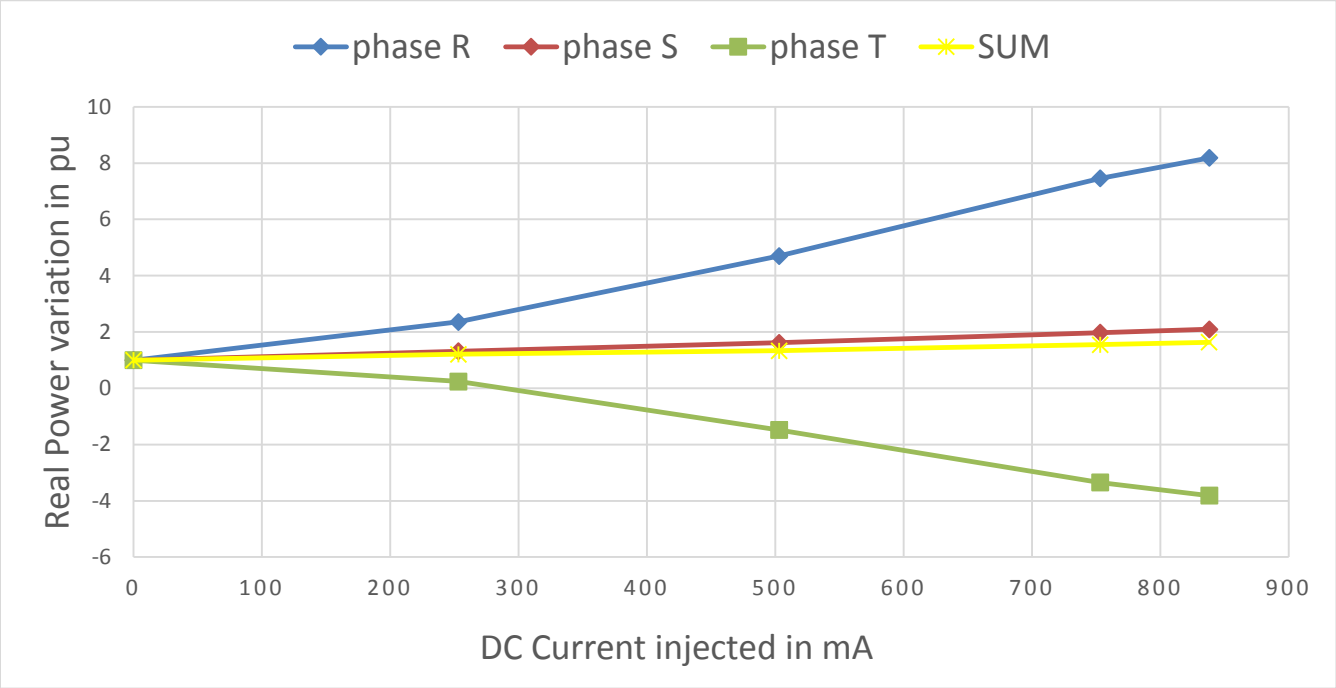

Figure 50: Real power consumption in Transformer 1 against DC current injection when no resistance is set in phase S

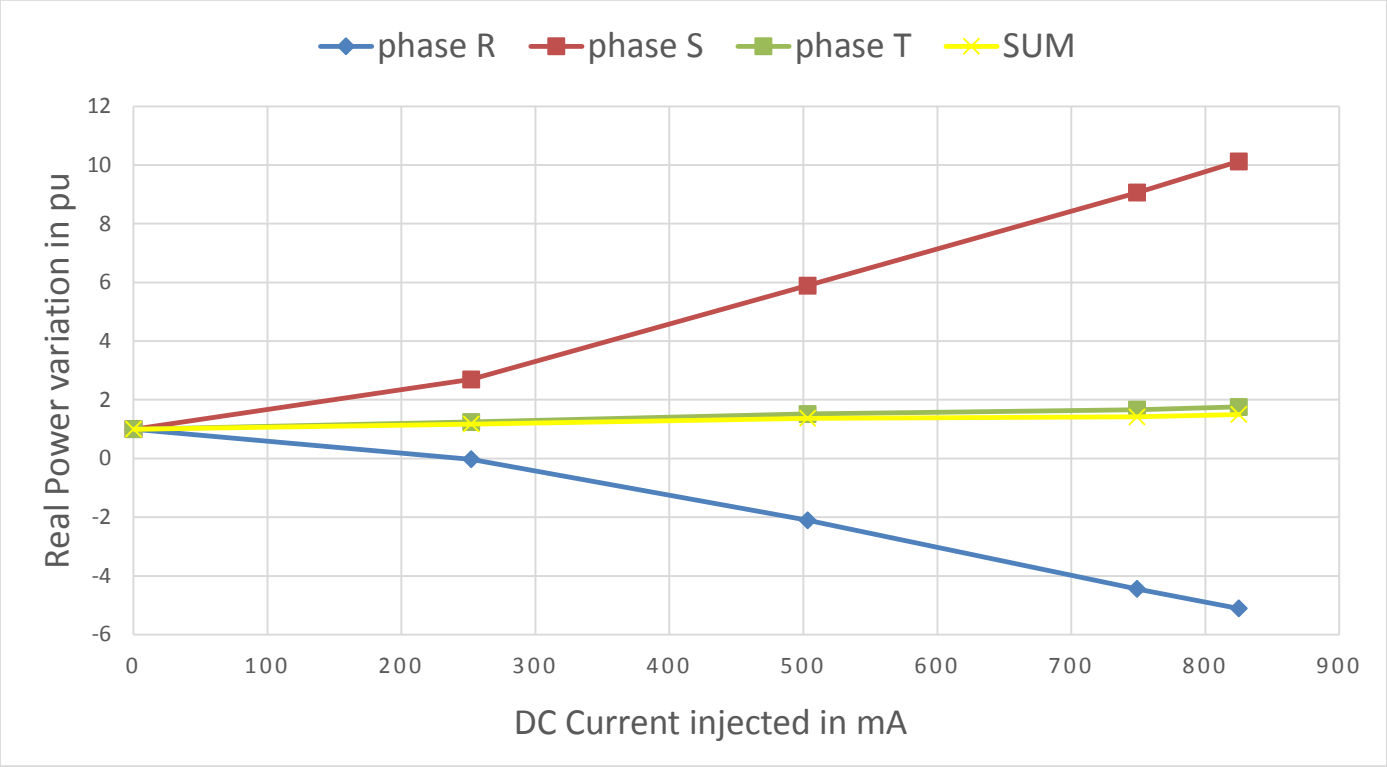

Figure 51: Real power consumption in Transformer 1 against DC current injection when no resistance is set in phase T

As a first approach, it can be said that the three scenarios follow the same trend: an increase of approximately 150 % in the total sum of the real power consumption is observed. Furthermore, there is always one phase that increases its power consumption, as the DC injection increases, and the other one, which shows a decrease of it.

When the unbalanced current is induced to flow through phase R, is phase T power the one that rises with the DC, and phase S, the one that see reduced its value. When the unbalanced situation is induced in phase S, is now phase R which rise his power, and phase T which decreases it. Phase S is eventually the one which increases its real power consumption, when an unbalanced situation is induced in phase T, and phase R the one which shows a decrease on it. As a sum up, it can be said that the three phases distributes the power in a way, that the sum of the power of the three phases remains always positive.

The computed real power values for Transformer 2 follows exactly the same behavior, although the total sum of Transformer 2 decreases in a significant way, as the DC injected current is positive for one transformer, but negative for the other.

Concerning the apparent power consumption S, it can be found how it follows the same trend as the currents of Figure 45-47. Figure 52-Figure 54 show for the three unbalanced scenarios the computed powers for both transformers.

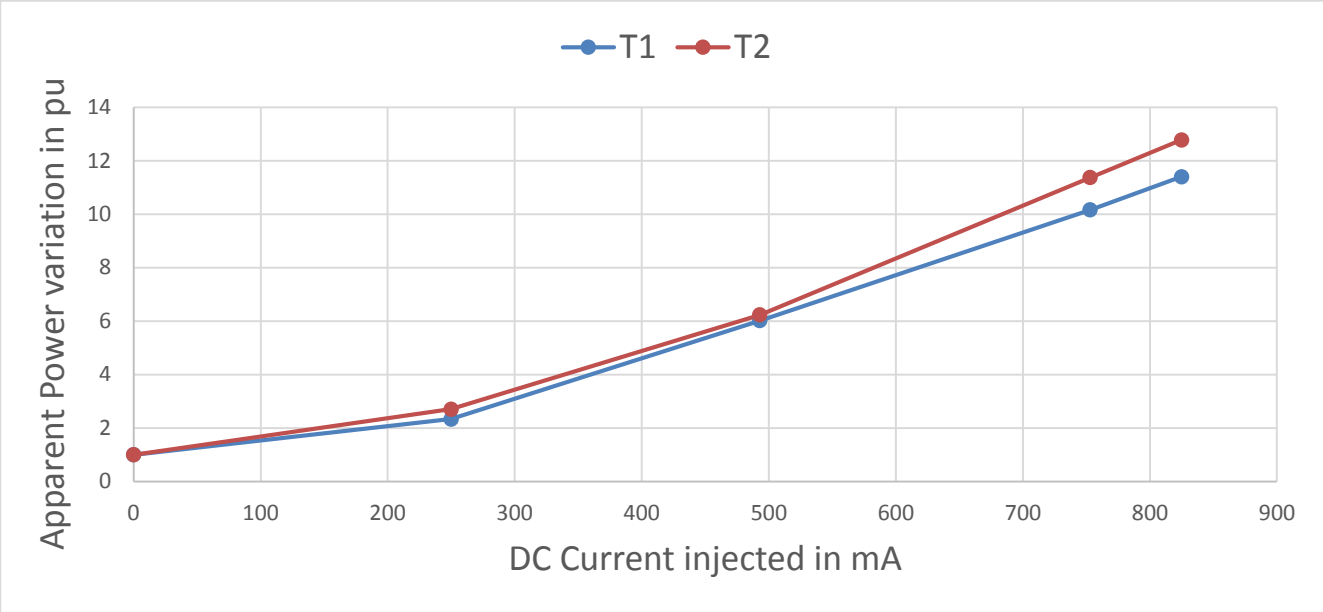

Figure 52: Power consumption against DC bias when an unbalanced case is induced in phase R

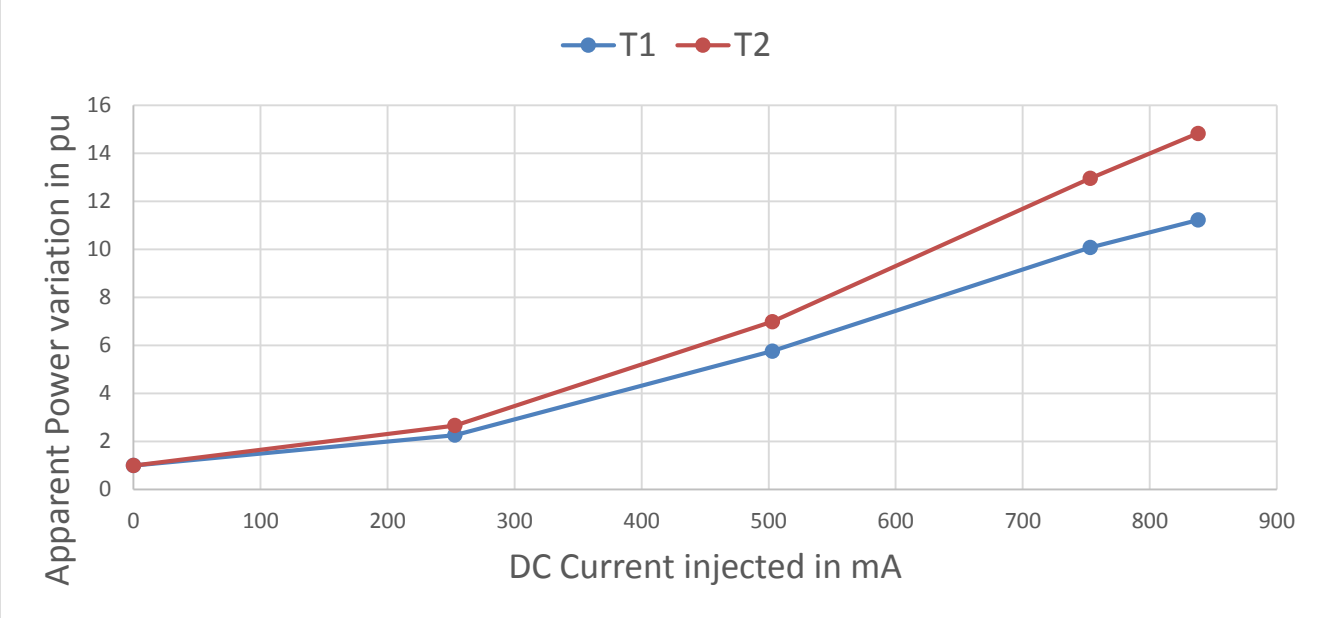

Figure 53: Power consumption against DC bias when an unbalanced case is induced in phase S

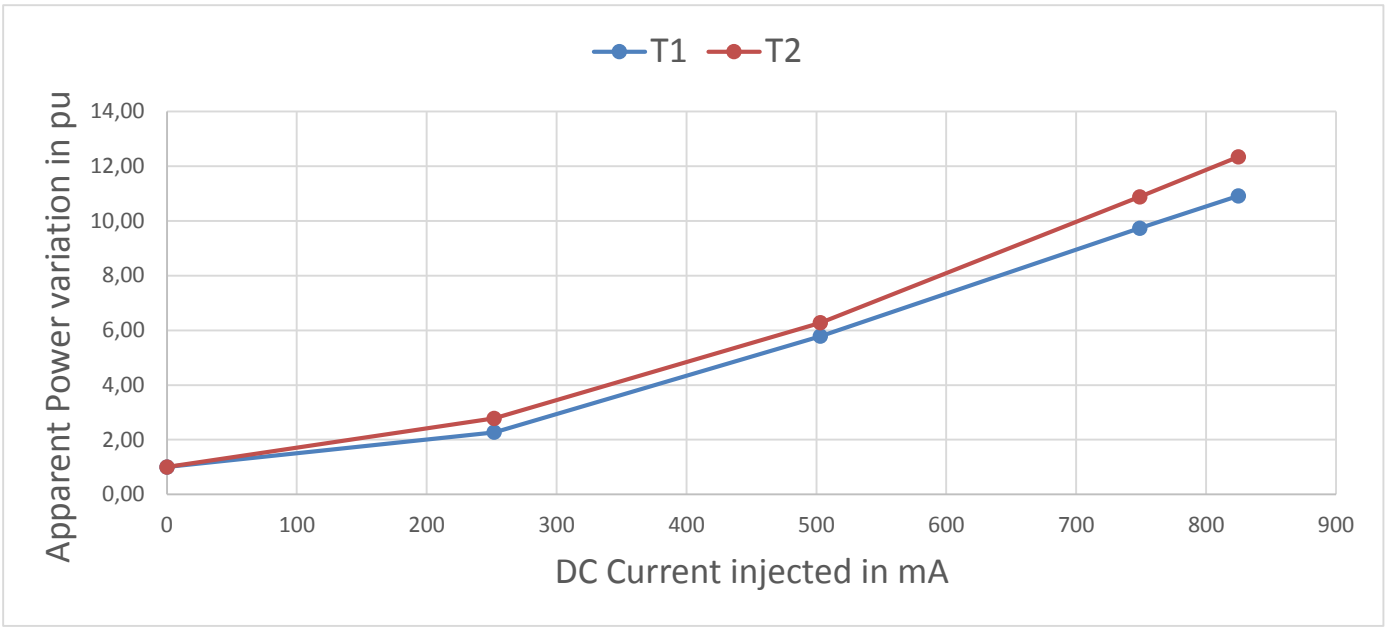

Figure 54: Power Consumption against DC bias when an unbalanced case is induced in phase T

The reader can notice that the three graphs follow the same trend. It is interesting to notice that, under DC injection, the total power that demands the setup rises significantly, reaching even 12 times the value without DC, when the unbalanced case is induced to phase R and phase T, and 14 times for phase S. The unbalanced phase through which the greater current flows in each case, contributes the most to the total power, as can be seen in Figure 55.

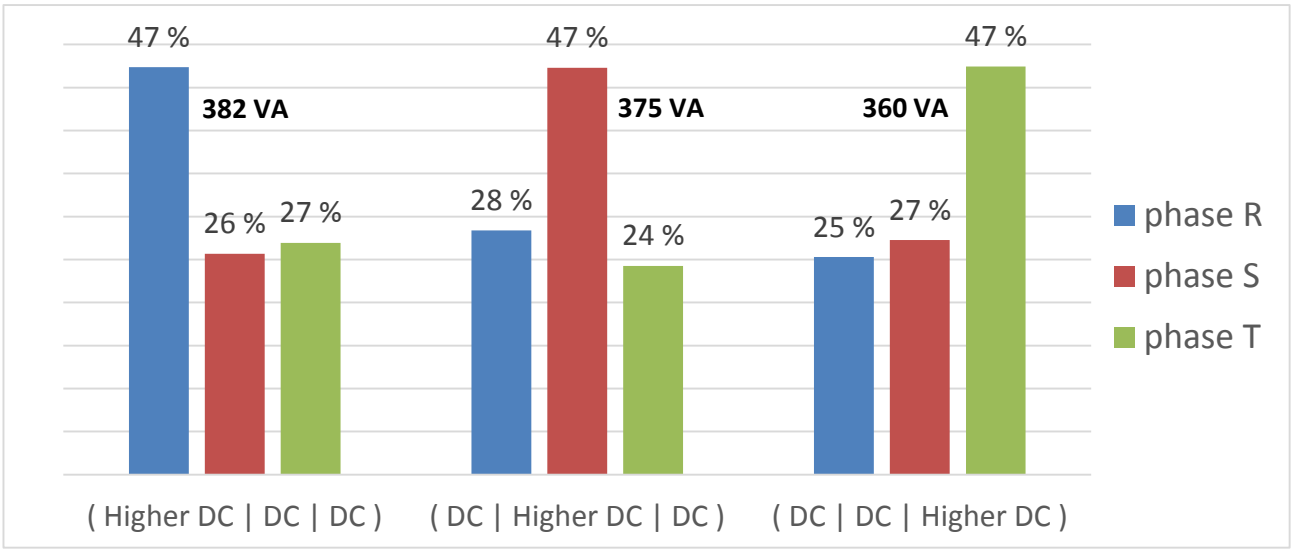

Figure 55: Contribution in % of each phase to the total apparent S when high DC in injected separately in each of the three phases

The rising rate of these powers is ruled by the level of saturation that show the transformers. From a 250 mA DC injection to 500 mA, the transformer starts getting into saturation, as the permeability μ of the iron core start to decrease. The currents show therefore an increase, and so does the power.

6.3 DC Comparison between real measurements and model simulations

The DC setup used along this thesis has been implemented in the MATLAB model in the way shown in Figure 56.

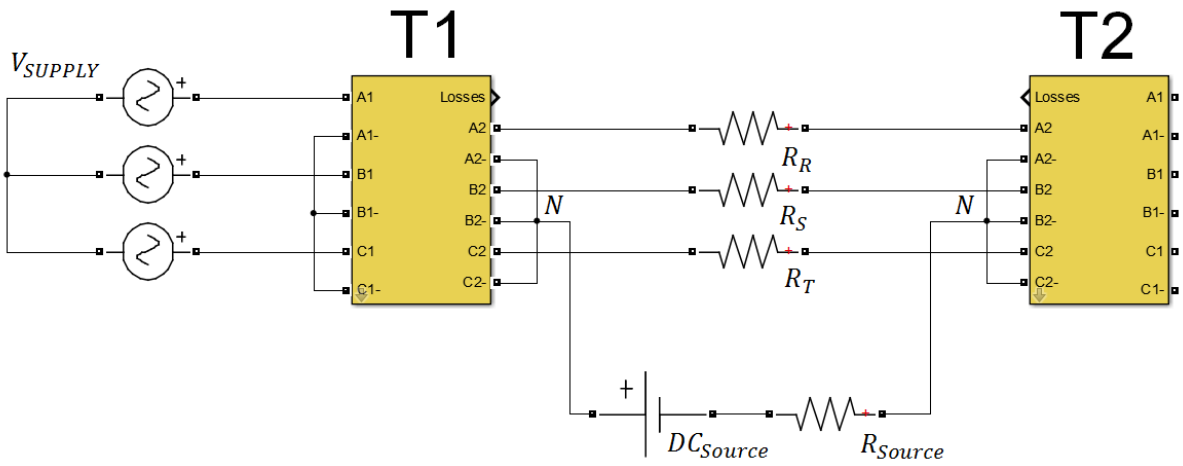

Figure 56: MATLAB model scenario for DC behavior analysis

As introduced at the beginning of this chapter, the chosen scenario consists of two transformers in series, and a DC current source, which injects a DC current through the secondary neutral points of Transformer 1 and Transformer 2 by means of 1 Ohm resistances, set in each phase.

The not-perfectly balanced voltage supplied by the step-up transformer, as well as the DC current source and the asymmetries present in the real transformers used in the setup introduce an error that must be taken into account for the results.

Different simulations for 500 mA (referred as medium level) and 850 mA (referred as high level) of injected DC are carried out with the parameters shown in Chapter 4, for the balanced case as well as for the unbalanced. The comparisons between simulations and measurements are made in two locations of the setup: before the first transformer and before the second one.

6.3.1 Balanced case

The iron cross section was introduced in the model following the computation shown in Section 3.4.

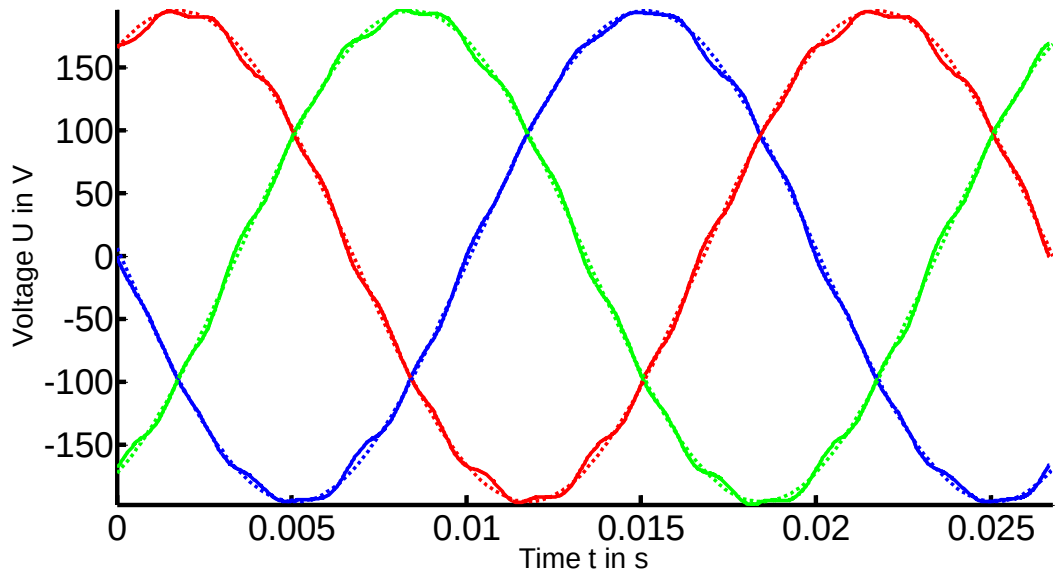

Figure 57: Voltages comparison before Transformer 1 between model and measurements for a medium level of DC.

It can be seen that both the simulated currents and the measured ones match well to each other. However, the behavior is not completely identical.

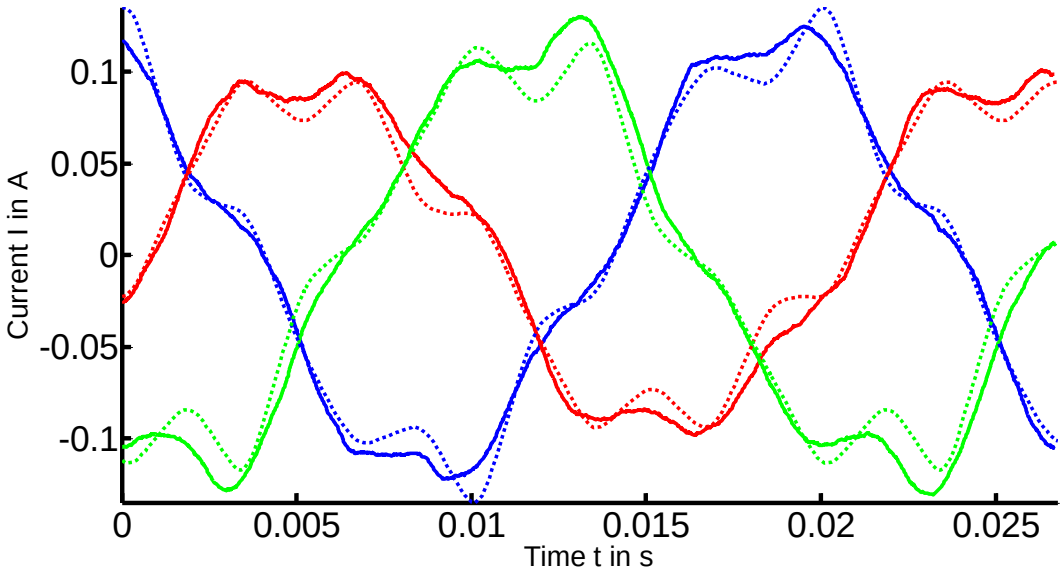

Figure 58: Currents comparison before Transformer 1 between model and measurements for a medium level of DC.

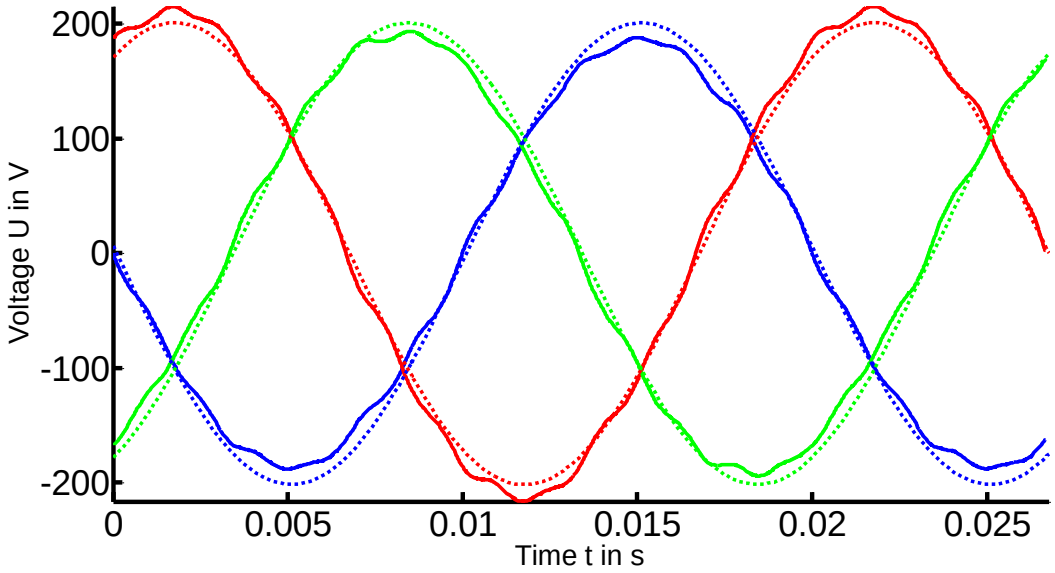

Figure 59: Voltages comparison before Transformer 2 between model and measurements for a medium level of DC.

In Figure 59 it can be seen the tendency of the output voltage of Transformer 1, mentioned in the previous sections. The central phase increases its voltage, while the other phases decrease it.

Same tendency as in Figure 58 can be seen in Figure 60, for the currents of the second transformer.

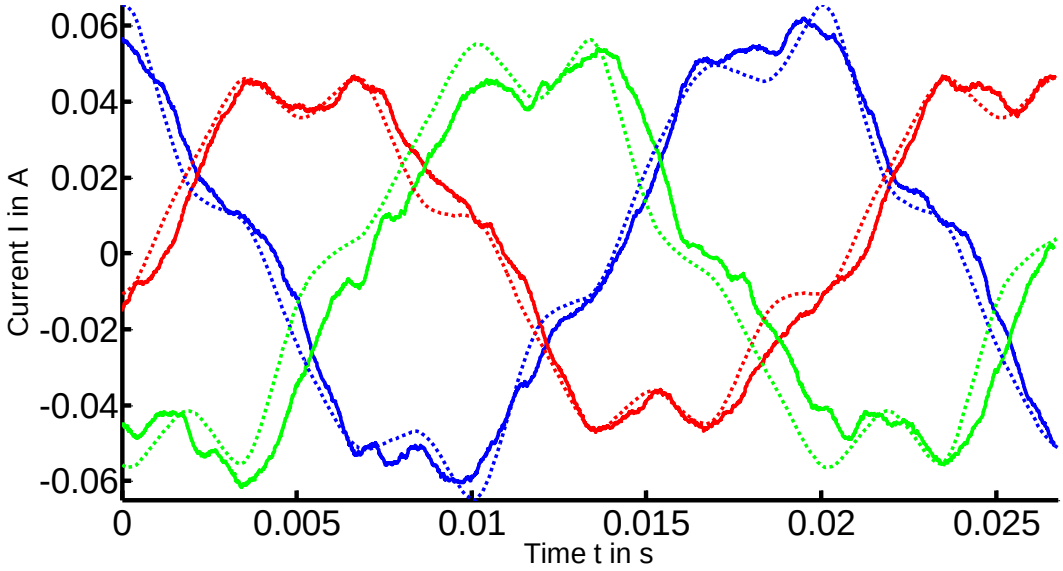

Figure 60: Currents comparison before Transformer 2 between model and measurements for a medium level of DC.

When a higher level of DC is applied, both model and measurements follow exactly the same behavior as for the figures shown above. Regarding the amplitudes, they remain as well unchanged, as shown in Section 6.1.

6.3.2 Unbalanced case

When the injection is carried out for different levels of DC, it can be seen how in the phase where the unsymmetrical case is induced, more current is flowing due to the lower DC impedance. However, in the other phases not the same amount of current is flowing. The distribution of the DC current among the different phases is ruled by the load, which is in this case the two transformers. In addition to the inherent asymmetry of the central phases, the external phases are not perfectly symmetrical, as was said before, due to several construction differences, i.e. the numbers of turns, the disposition of the iron core and the geometry. Due to this asymmetries, it can be expected that the DC currents flowing through each phase are also different.

It is remarkable to say that these asymmetries are unknown, and therefore cannot be implemented in the model. The DC current flowing through the balanced phases are very similar in the simulations, while not in the real transformer. This fact is believed of high relevance, in order to judge the results.

Simulations were carried out for different levels of DC with the same parameter for the iron cross section than the one used for the balanced case. The model response was not satisfying, as the model transformers went into a much higher level of saturation than the ones at the real setup. However, this was an expected event this time. A greater flux offset than in the balanced case is flowing now through the iron core, and therefore, this greater magnitude of flux must cover a bigger section inside the iron core, according to the explanation given in Section 3.4. In order to set the proper cross section in the model, the computations shown in Section 3.4 are taken into account, and an analysis of the fluxes flowing during the simulations for different levels of DC is carried out. In the outline of this work (Chapter 7), a more accurate calculation for this matter is proposed.

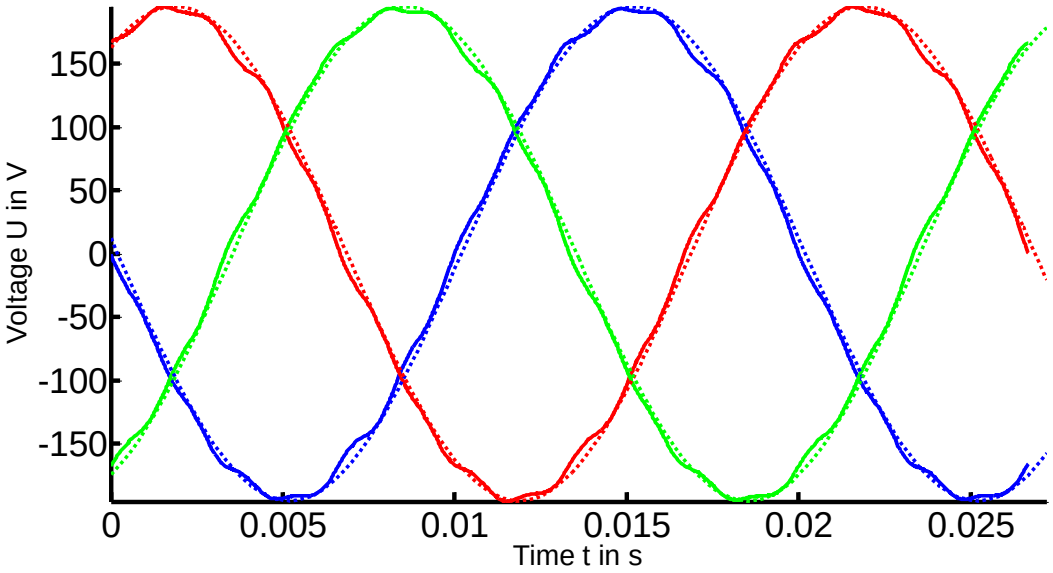

Figure 61: Voltages comparison before Transformer 1 when the unbalanced case is induced in phase R for a medium level of DC.

In Figure 61-Figure 64 can be seen that the model adjusts well to the real behavior, although the model has a quicker response at the saturation peaks. The differences on the way the saturation peak rises its value, on the way the transformer gets in and out of the saturation region can also be caused by small differences between the BH curve implemented in the model and the real one.

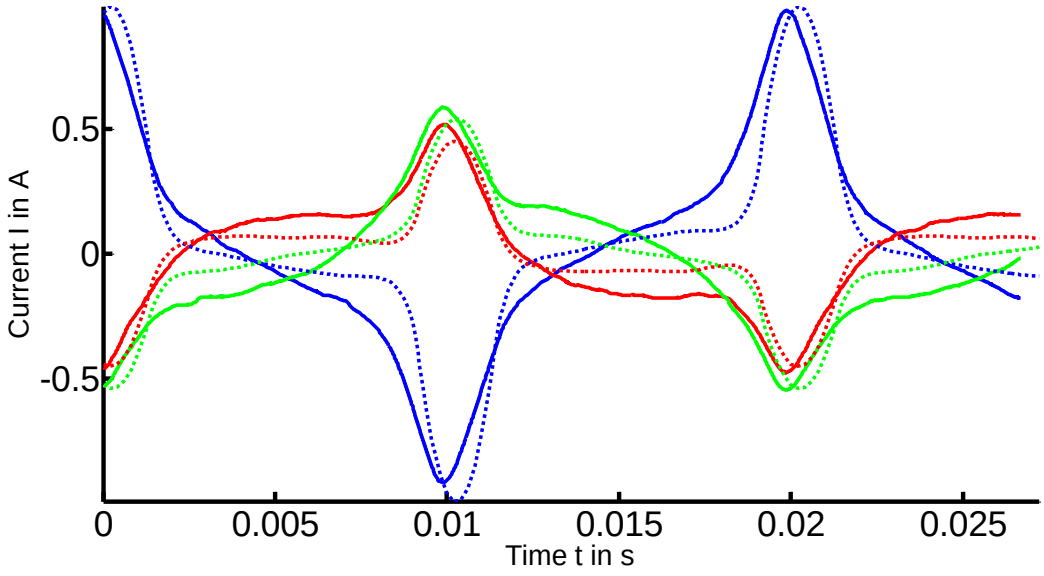

Figure 62: Currents comparison before Transformer 1 when the unbalanced case is induced in phase R for a medium level of DC.

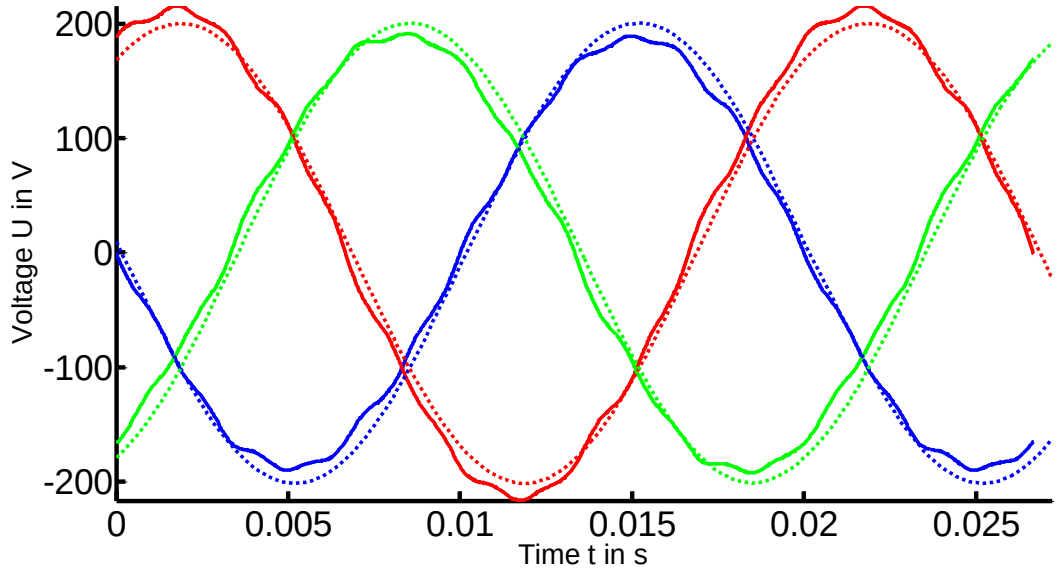

Figure 63: Voltages comparison before Transformer 2 when the unbalanced case is induced in phase R for a medium level of DC.

The same increasing/decreasing tendency as the one seen for the balanced case is observed in the voltage of Transformer 2 for the unbalanced case.

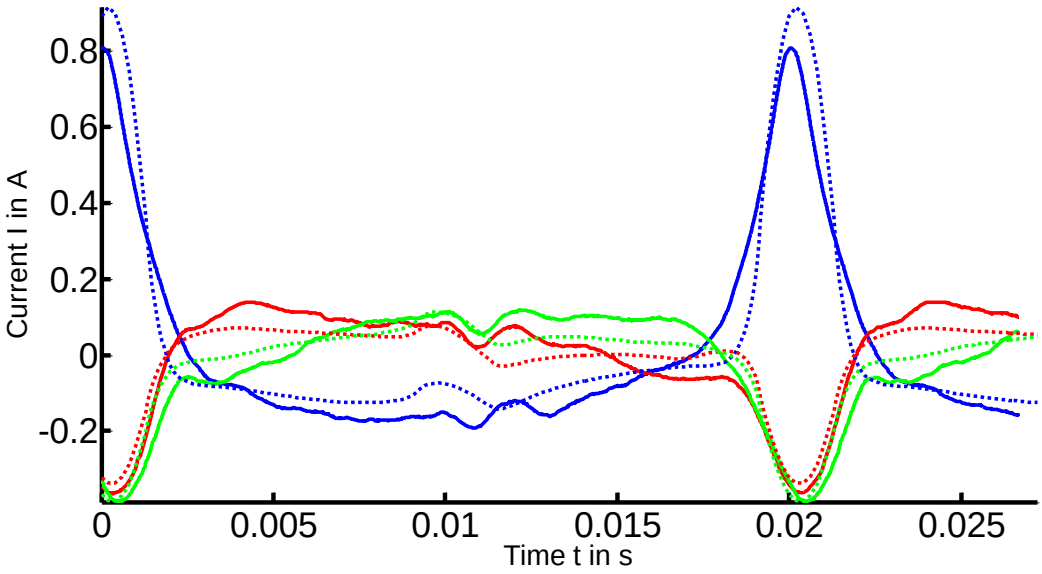

Figure 64: Currents comparison before Transformer 2 when the unbalanced case is induced in phase R for a medium level of DC.

An appreciable discrepancy is observed in Figure 64 in the portion of waveforms between the saturation peaks. It can be seen that the model does not follow completely the changes in the current of the real transformer. These variations are checked to be caused by the zero-sequence return flux. The excitation currents associated to this flux that flows through the neutrals conductor differ between the model and the real measurements. As the system gets more and more unbalanced with the DC injection, the zero-sequence flux and therefore the

zero-sequence currents increase their value, having a bigger effect on the magnetization currents.

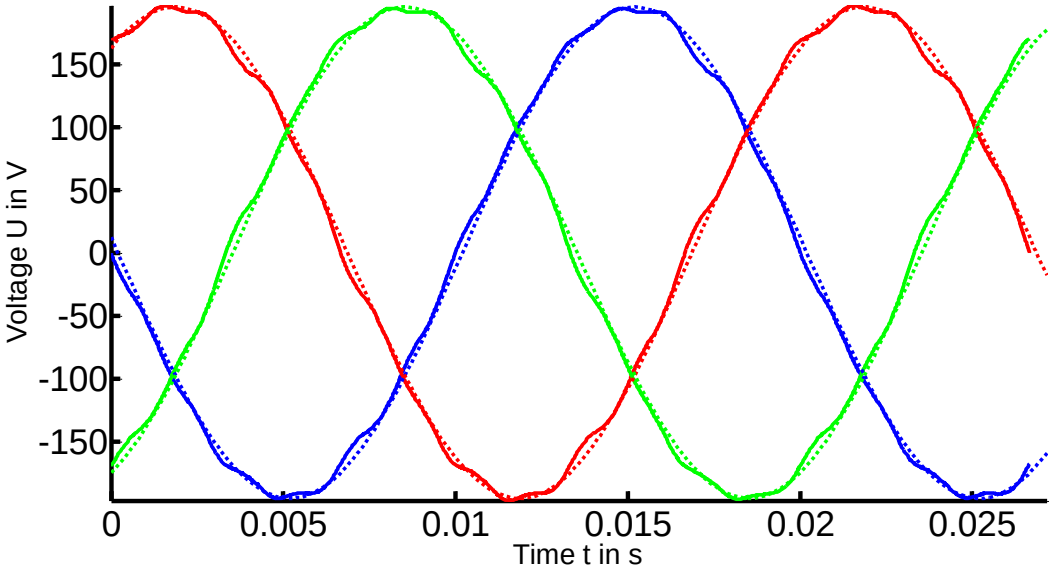

Figure 65: : Voltages comparison before Transformer 1 when the unbalanced case is induced in phase R for high level of DC.

When the transformer is at full saturation, under high DC, high excitation currents are achieved (up to 1.7 A), and the same behavior is observed between the model and the real transformer, as show Figure 65-68.

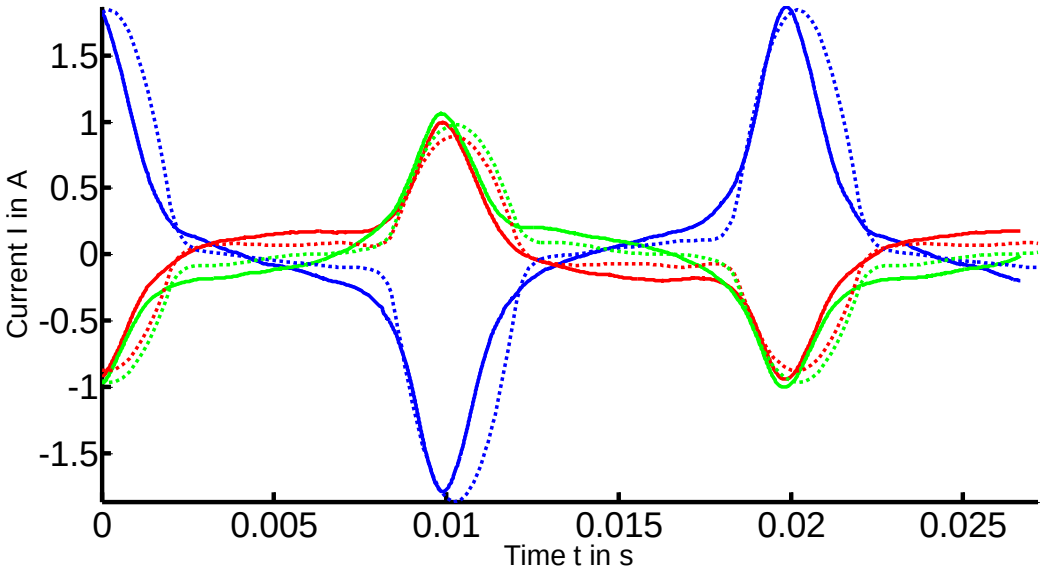

Figure 66: Currents comparison before Transformer 1 when the unbalanced case is induced in phase R for a high level of DC

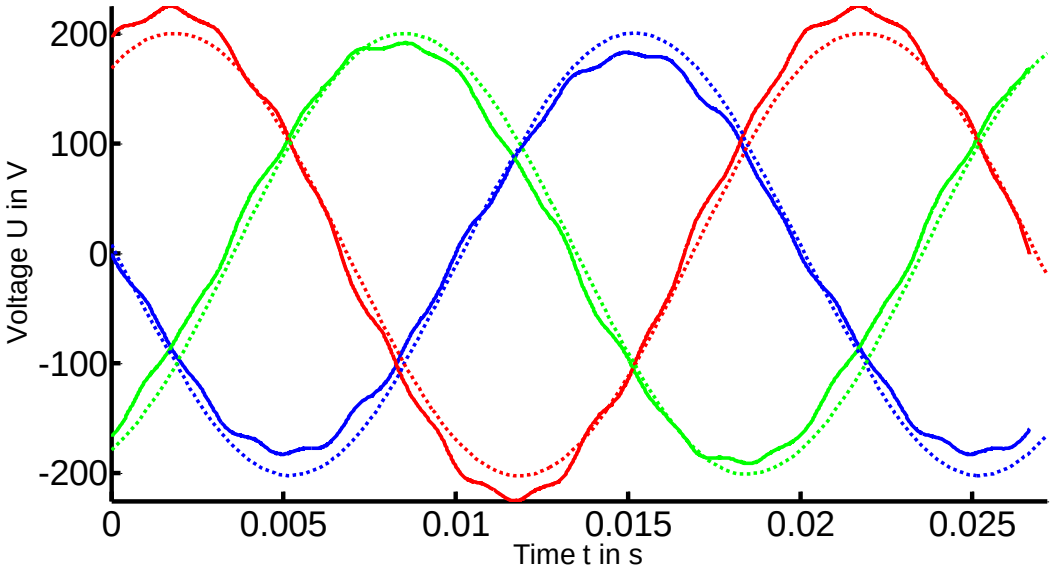

Figure 67: Voltages comparison before Transformer 2 when the unbalanced case is induced in phase R for a high level of DC.

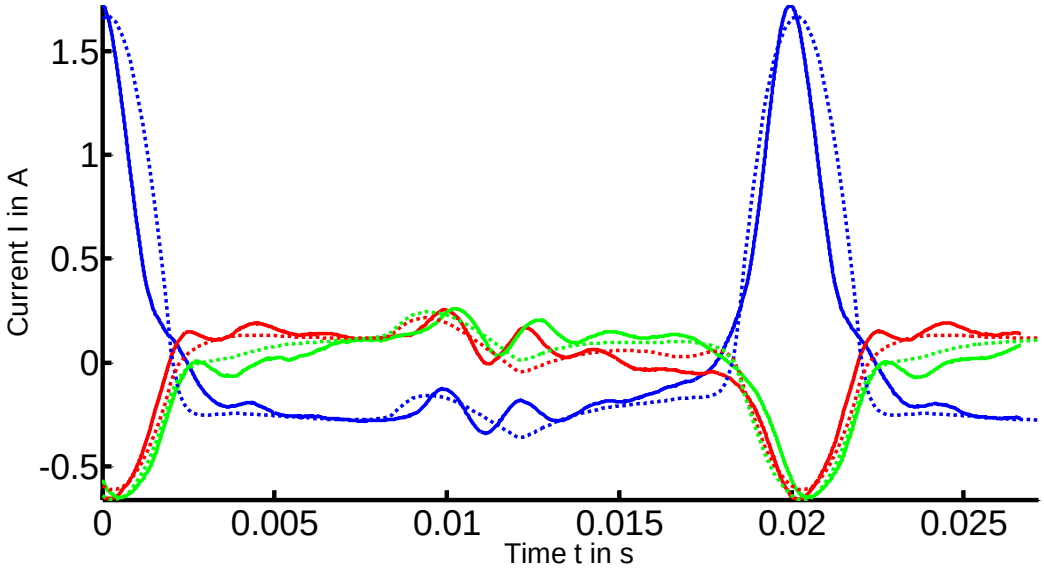

Figure 68: Currents comparison before Transformer 2 when the unbalanced case is induced in phase R for high level of DC

When the unbalanced case is induced in phase S, the current of this central phase reach a peak due to saturation. In the measurements done for all levels of DC can be seen that phase R delivers always more current than phase T in order to compensate this extra-current due to

saturation. This phenomenon, which reflects the asymmetry present in the real transformer, is not perfectly integrated in the model, and is considered therefore as a limitation.

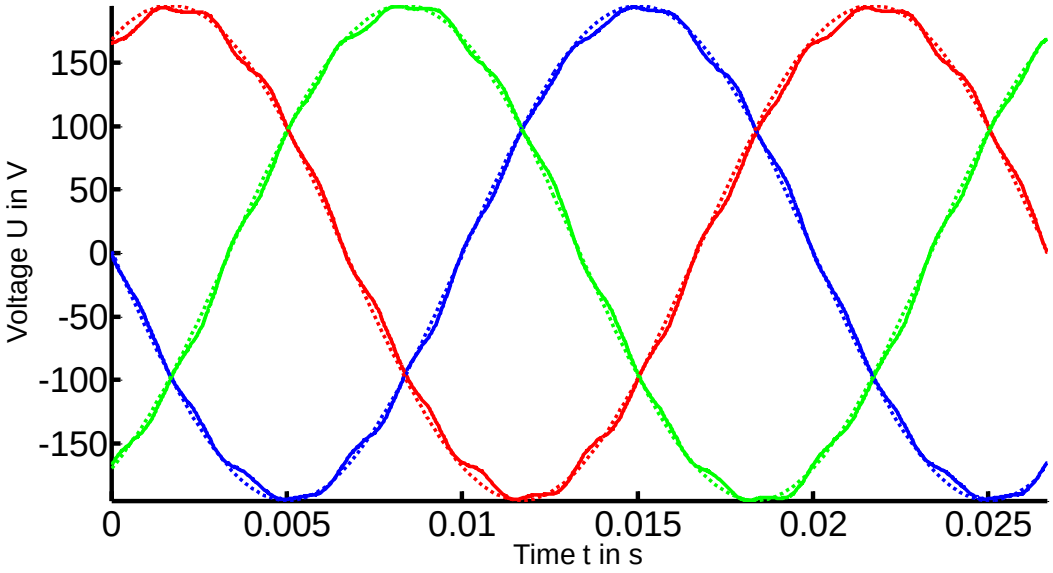

Figure 69: Voltages comparison before Transformer 1 when the unbalanced case is induced in phase S for a medium level of DC

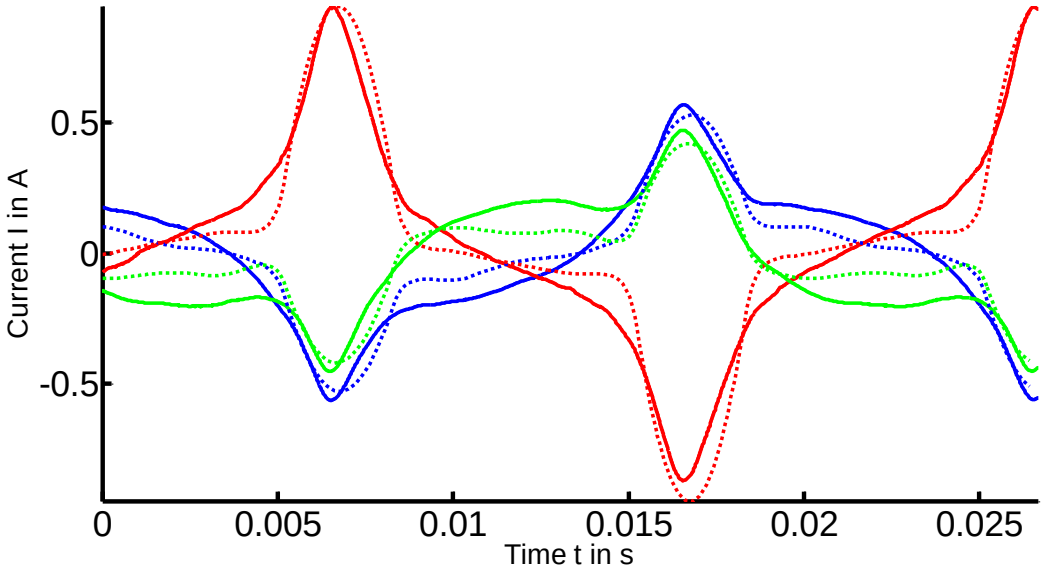

Figure 70: Current comparison before Transformer 1 when the unbalanced case is induced in phase S for a medium level of DC.

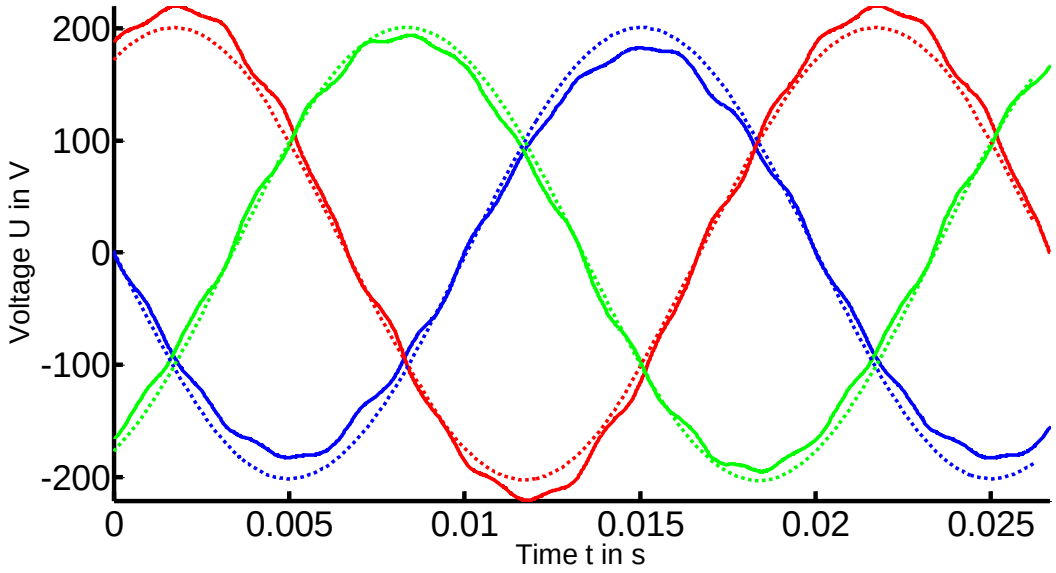

Figure 71: Voltage comparison before Transformer 2 when the unbalanced case is induced in phase S for a medium level of DC.

Under high DC injection, high excitation currents are achieved (up to 1.7 A), and the same behavior is observed between the model and the real transformer.

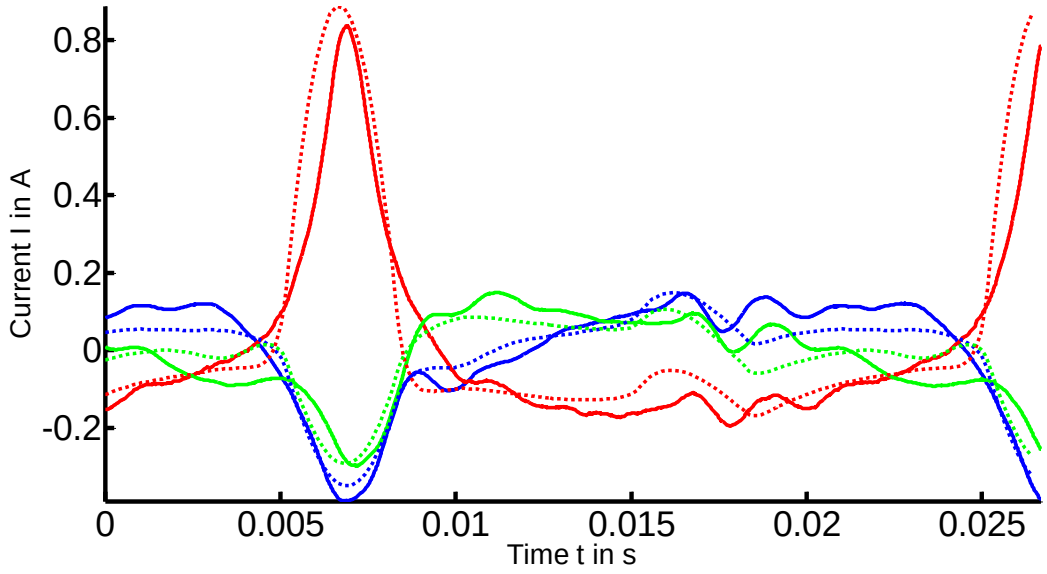

Figure 72: Current comparison before Transformer 1 when the unbalanced case is induced in phase S for a medium level of DC.

For the remaining external phase (phase T), similar behavior as for the unbalanced case in phase R is observed.

Regarding the real power consumption, a comparison between model and real setup is made in Figure 73 and Figure 74 for a medium (500 mA) and high (850 mA) level of DC. The power losses computed for the real setup are taking into account the iron losses as well as the copper losses. In order to proceed in the same way with the model, the power losses are computed

this time by multiplying the simulated voltages and currents, and not as explained in Section 1.3, though the magnetic density value B.

In both graphs it can be seen that the losses for zero DC injection are very close to the ones when a symmetrical DC is injected in all phases. This result was already seen in Section 6.1.

The losses provided by the model, however, result for the unbalanced cases slightly lower than the ones of the real setup. These differences, however, can be expected. Manufacturers define during the transformer design a "building factor", which takes into account additional losses that can arise due to overlaps in the iron core and changes in the magnetic flux density at the corners of it. These differences can be expected to be greater when the transformer is under high saturation, which occurs in the unbalanced cases.

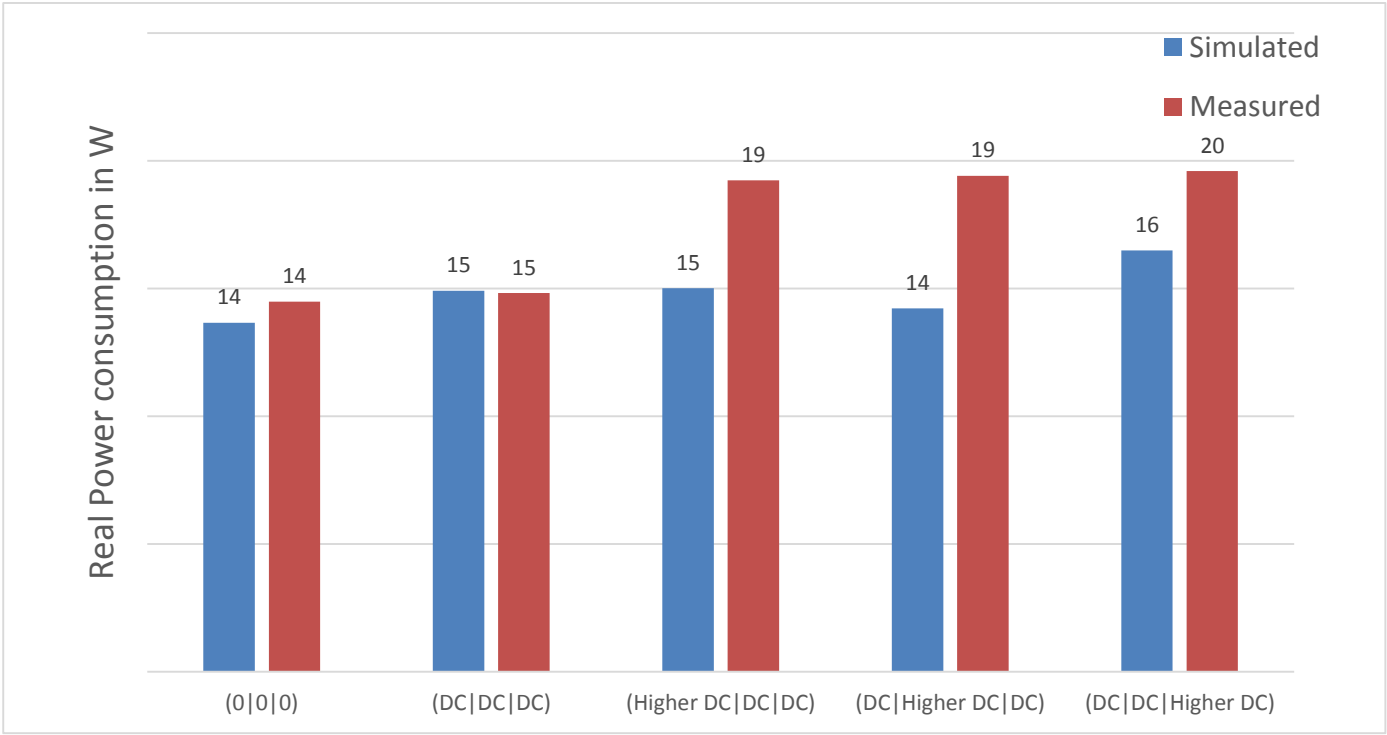

Figure 73: Real power comsumption of model and real setup for a medium level of injected DC

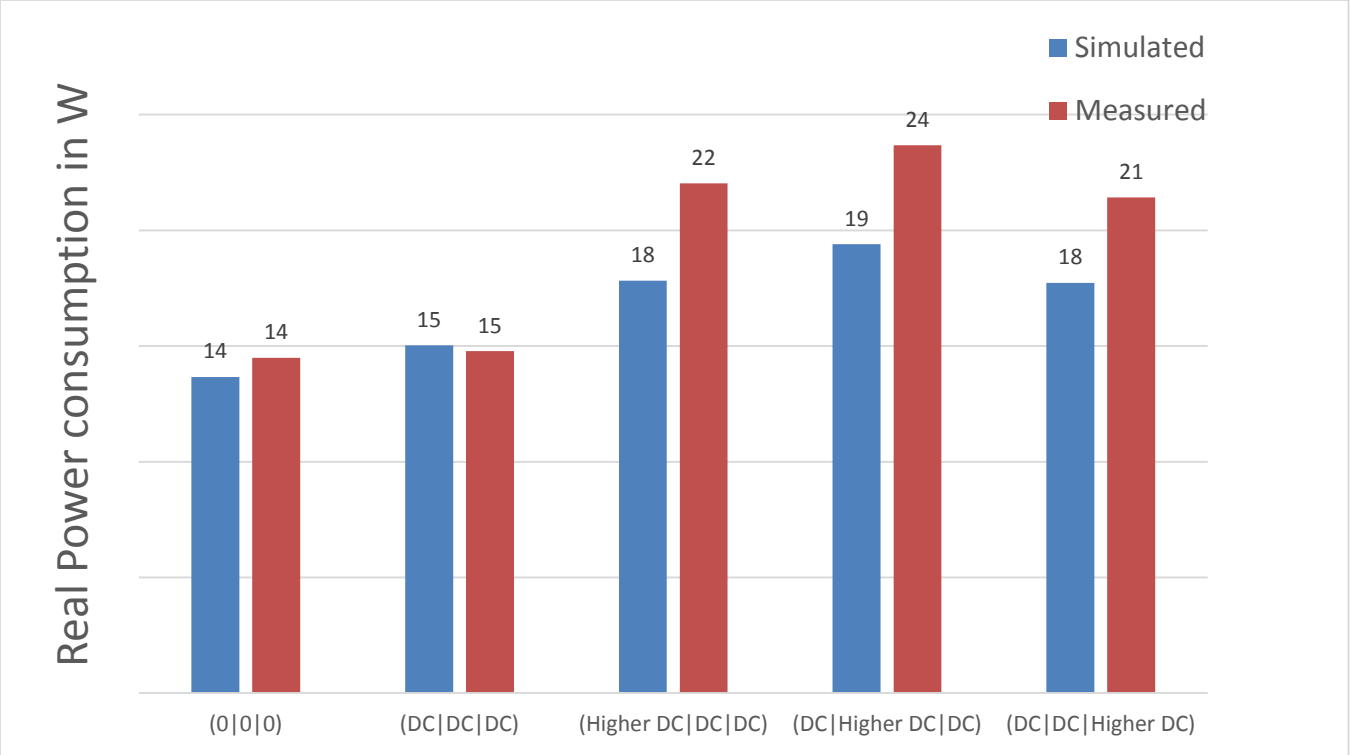

Figure 74: Real power comsumption of model and real setup for a high level of injected DC

7 Sum-up and future works

In this work, an investigation of the effects of DC components on transformers and the power network is carried out. For this purpose, a development of a laboratory setup and a detailed analysis of the measurement results is made. As a next step, the behavior of the MATLAB-Simulink model is successfully verified with the experimental data.

However, several limitations are noticed in the model during the process. The real transformer shows an asymmetrical behavior due to non-ideal construction, which the model does not take into account. In order to reduce these differences and achieve a more realistic model, several modifications are made. These asymmetries are, however, not known in detail and cannot be implemented into the model. Therefore, further investigation should be made towards this purpose.

Simulations are carried out firstly under nominal operation, once the proper parameters are set in the model, and a close response compared to the real measurements is obtained.

An analysis of the behavior of a setup composed of two transformers under direct components is examined. In first place, a symmetrical current is injected in the three phases, and no effects are observed for different levels of DC. However, when an unbalanced case is induced, the power losses go up to 163% in some cases, and 1300% of apparent power is demanded from the network by the setup. High peak currents and a deep level of saturation is observed during the measurements and simulations.

As a next step, a validation of the model is made throughout a detailed comparison with the experimental data, obtained during the DC analysis.

Several matters are highlighted below, as a guidance for future works:

- As seen along this thesis, the model seems to respond quicker than the real transformer to sharp variations on the currents, as happens at the saturation peaks. The model used in the simulations does not take into account the mutual inductances between phases, which determine how this response is. This is considered as a limitation of the model and is left to further investigation.

- Due to the different iron core covered section observed on the real transformers depending on the flux flowing through them, an interpolation function by means of a look-up table can be implemented in the Simulink model.
  This look-up table would provide an iron-cross section depending on the flux flowing inside the iron core, and it would be built carrying out identical calculations as the ones shown in Section 3.4, but for a wider range of fluxes. Several simulation tests could be

performed in order to obtain the most suitable section, leading to an iteration process, since the cross section also affects on the flowing flux.

- Further investigation on the main asymmetries present on transformers, and a way of implementing them in the MATLAB model, can be useful in order to obtain more reliable simulations.

- A more complete analysis of the transformer under DC component can be carried out. The response of the transformers during parallel operation, under different connections to the network and different load conditions can contribute in order to get a wider knowledge of the effects of the DC. A harmonic analysis through a FFT function applied on the voltages and currents under the effect of direct components could be also of high interest.

8 Appendix

8.1 Initialitation MATLAB code for reactances

```
x1=urx1(3)/2; % urx1 (3) is the per unit short-circuited voltage
x2=x1;
L1=x1*u1^2/pnom/(2*pi*fnom); % leakage reactance winding 1
```

8.2 Integration MATLAB code for flux ϕ and flux density B calculations

```
%% Voltage integration, Flux calculation.

timestep = Data_Offset_Corr(2,1)-Data_Offset_Corr(1,1);
samples = 1/timestep;
i=1;
while Data_Offset_Corr(i,2)*Data_Offset_Corr(i+1,2)>0  % i such that v1(i)=0;
    i=i+1;
end
i

t1=Data_Offset_Corr(i:i+round(2*samples/frequency),1); %Takes a vector of 2T
time from the data and 2T voltages
v1=Data_Offset_Corr(i:i+round(2*samples/frequency),2);
i1=Data_Offset_Corr(i:i+round(2*samples/frequency),3);

i=1;
m=1;
a=5; %integration step
while i<round(2*samples/frequency)-a  %Integration over 2T
t2=t1(i:i+a);
v2=v1(i:i+a);
i2=i1(i:i+a);
deltaflux(m,1)=trapz(t2,v2); %trapezoidal integration method.
tfinal(m,1)=t2(a+1);
i3(m,1)=i2(a+1);
i=i+a;
m=m+1;
end

k=length(deltaflux);

flux(1)=deltaflux(1,1);
for j=2:k  %Incremental variations are added to the previous ones, in order
to get the integral function.
    flux(j)=flux(j-1)+deltaflux(j,1);
end

flux=[0,flux];
%i3=[i3(1);i3];
tfinal=([t1(1);tfinal])';

Offset_flux = mean(flux);  %Supposing no Flux Offset.
flux=(flux-Offset_flux);
```

```
N1=277;
N2=286;
rt=277/286;

%phi_0=-325.464/(2*pi*frequency*rt); %Initial Condition: t=0; x=0;
%Fluxfinal=Flux+phi_0;

flux=flux./N2;
A=0.0019750; %Cross section Limbs
B=flux./A;

L=0.17328; %Average Lenght of the Limb
H=i3.*(N1/L);

figure
plot(tfinal,flux,'b');
figure
plot(tfinal,B,'k');

H1=H(1:length(H)/2); %B-H Curve plotted over T, not 2T
B1=B(2:(length(B)+1)/2);
H1B1=[H1 B1'];

figure
plot(H1,B1);
```

8.3 Peak magnetic polarization against Peak magnetic field strength.

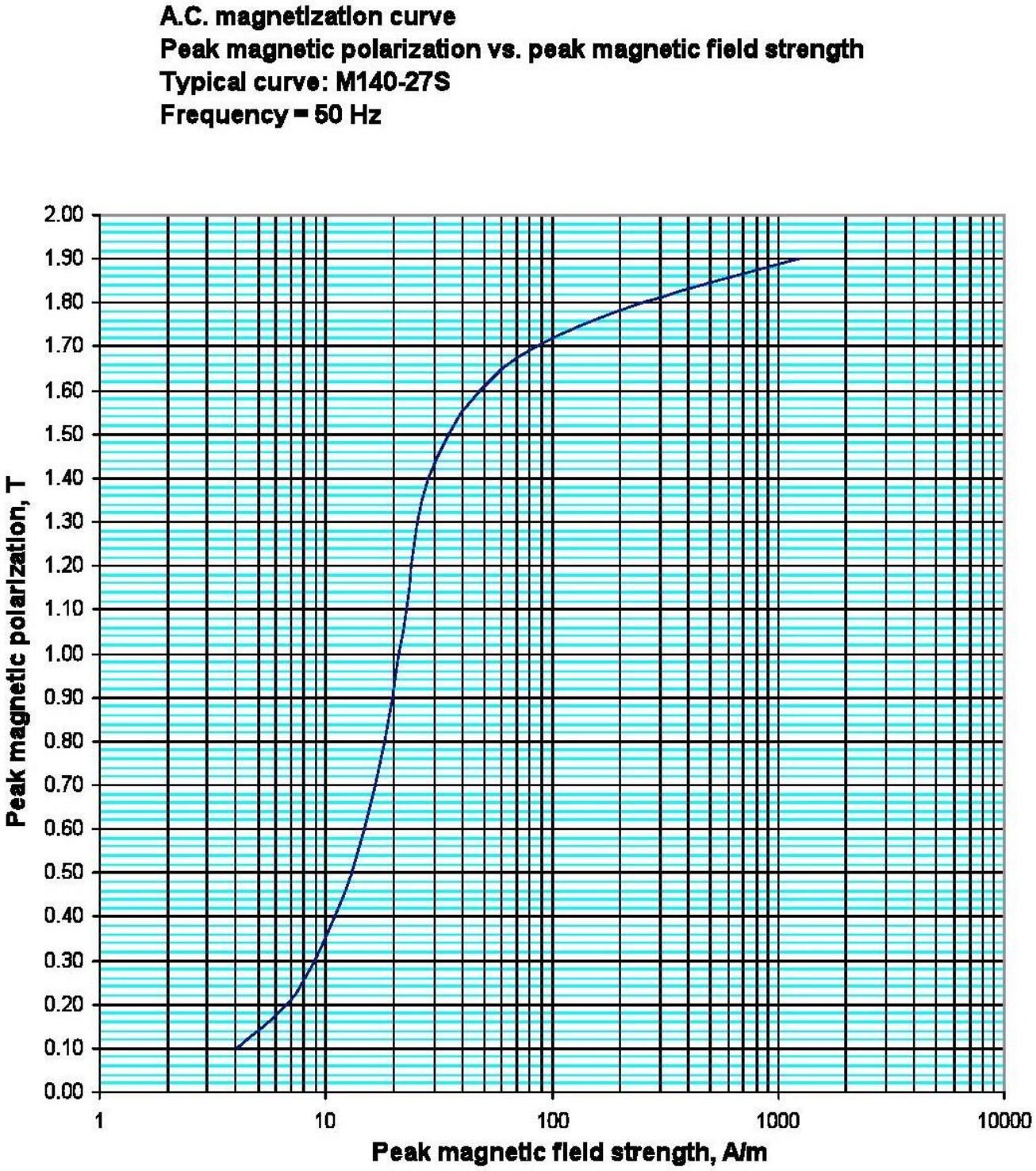

Figure 75: Peak magnetic polarization against peak magnetic field strength manufacturer data sheet

8.4 BH implemented curve in the model

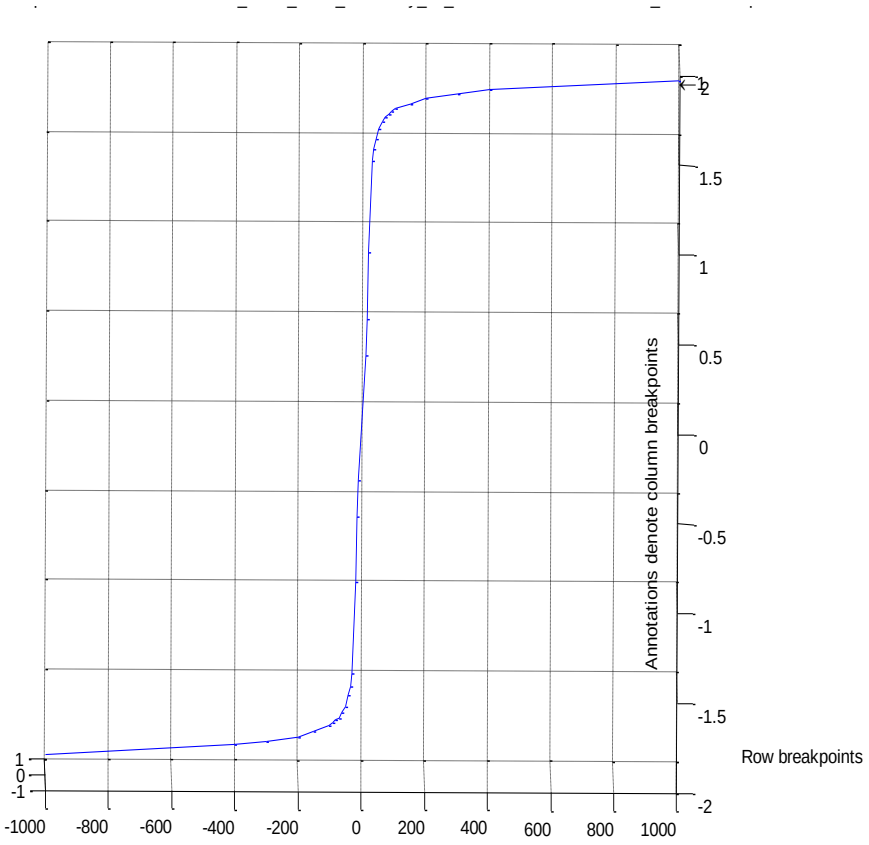

Figure 76: BH implemented Curve taken from the manufacturer data sheet.

9 Index of literature

1) http://www.cogent-power.com/unisil/typical-properties/
2) *Kulkarni SV, Khaparde SA*. Transformer engineering. Design and practice. New York: Marcel Dekker, Inc., 2004
3) *Harlow JH*. Electric power transformer engineering. Boca Raton: CRC Press/Taylor & Francis, 2012; 3. Auflage
4) *Escarela Perez, Kulkarni et al 2007.* Asymmetry during No-Load loss measurement
5) *Haluk Odoglu.* BEST Transformer Tests, June 2009 (3th Edition).
6) *Mario Gnädig.* Untersuchung des Transformatorverhaltens bei Gleichstromeinkopplung in Wechselstromübertragungsleitungen, 2013
7) *Ashley Karl Zeimer.* The effect of DC Current on Power Transformers, October 2000
8) *Philip Marketos, Antonhy J. Moses, Jeremy P.Hall*. Effect of DC voltage on AC magnetisation of transformer core steel. Journal of Electrical Engineering, 2010.
9) *Matti Lahtinen, Jarmo Elovaara*. GIC ocurrences and GIC Test for 400kV system transformer. Power Delivery, IEEE Transactions on 2002; 17: 555–561
10) *R*. Girgis, Fellow, k. Vedante. Effects of GIC on Power Transformers and Power Systems. IEEE 2012
11) *Poria G*. Khorasami, Ali Dehimi. A new Modeling of Matlab for accurate Simulation of Ferroresonance. Powereng 2009.
12) *Bruce A*. Mork, Francisco Gonzalez, Dmitry Ischenko, Don L. Stuehm, Joydeep Mitra. Hybrid Transformer Model for transient simulation – Part I: Development and parameters. IEEE Transactions on Power Delivery on 2007; 22: 248-254
13) *E. Mulasalihovic et al.* Effects of geomagnetically induced currents on the magnetic performance of transformer cores, JMMM, 320, 2008.
14) *Leon F de, Semlyen A*. Complete transformer model for electromagnetic transients. Power Delivery, IEEE Transactions on 1994; 9: 231–239
15) IEEE Recommended Practice for Establishing Transformer Capability When Supplying Non-sinusoidal Load Currents. [S.l.]: [s.n.], 1998
16) *Shu Lu, Yilu Liu*. FEM Analysis of DC Saturation to assess transformer susceptibility to GIC. Power Delivery, IEEE Transactions on 1994; 8: 1367-1375
17) *A. Krings, J. Soulard.* Overview and Comparison of Iron Loss Models for electrical Machines. KTH Royal Institute of Technology. Stockholm, Sweden.
18) *D.M.Said, K.M.Nor*. Effects of Harmonics on Distribution Transformers, 2008
19) *Y. Baghzouz, X. D. Gong*. Analysis of three-phase transformer no-load characteristics. IEEE Transactions on Power Systems on 1995; 10: 18-26
20) *Fiorillo F*. Measurement and characterization of magnetic materials. Amsterdam, San Diego, CA: Elsevier Academic Press, 2004; 1.
21) *T.Ngnegueu, F. Marketos, R.Xu, R. Bardsley, S. Barker, J. Baldaue, J. Oliveira.* Behavior of transformers under DC/GIC excitation: Phenomenon, Impact on design/design evaluation process and modelling aspects in support of design. Cigre 2012
22) *Bertotti G*. General properties of power losses in soft ferromagnetic materials. Magnetics, IEEE Transactions on 1988; 24: 621–630